CHALMERS

Modelling of sound transmission through multilayered elements using the transfer matrix method

Master's Thesis in the Master's programme in Sound and Vibration

KARIN TAGEMAN

Department of Civil and Environmental Engineering
Division of Applied Acoustics
Vibroacoustics Group
CHALMERS UNIVERSITY OF TECHNOLOGY
Gothenburg, Sweden 2013
Master's Thesis 2013:108

Modelling of sound transmission through multilayered elements using the transfer matrix method
Master's thesis in the Master's programme in Sound and Vibration
KARIN TAGEMAN
Department of Civil and Environmental Engineering
Division of Applied Acoustics
Vibroacoustics Group
Chalmers University of Technology

Abstract

A method in the framework of statistical energy analysis (SEA) is developed. The main purpose of the method is to characterise the sound transmission through multilayered structures.

The transmission factor of a multilayer is calculated with the transfer matrix method and spatially windowed to take the finite size of the structure into account. This transmission factor is used in the SEA model to estimate the coupling loss factors of two rooms separated by the multilayer.

The transmission factor is compared with available measurement data and it is concluded that the method gives good agreement for a thin plate. For a cavity wall, however, the method gives poor agreement with measurement data in the frequency range from the double wall resonance up to the critical frequency.

The SEA model is compared with existing SEA software. The result is similar for a thin plate, and it is proposed that this model gives a more detailed description of the power transmission.

Keywords: transfer matrix method, spatial windowing technique, statistical energy analysis, SEA, diffuse field, multilayer, stratified medium, sound power transmission factor

Acknowledgements

This master's thesis was written during the spring of 2013 as a part of the master's programme in Sound and Vibration at the Division of Applied Acoustics. The existence of the thesis is due to Patrik Andersson, who proposed the subject and has been my supervisor during the work. I would like to take the opportunity to express my gratitude to him. I would also like to thank Börje Wijk at the division and my husband for all technical support.

Karin Tageman, Gothenburg, August 2013

Contents

1 Introduction

The main purpose of this thesis is to investigate if the transfer matrix method can be used to improve modelling of multilayered structures with statistical energy analysis (SEA). Usually, the non-resonant transmission is described by the simple mass-law in SEA. With the transfer matrix method, a more detailed description of the transmission can be implemented to improve the result.

1.1 Structure of the thesis

To fulfil the main purpose of the thesis the transfer matrix method is evaluated together with the spatially windowing technique. The limitations and assumptions of the methods are investigated. Based on this, a MATLAB script that performs calculations of power transmission factor is designed, which is used within the SEA framework. This is validated and compared with existing SEA software. The structure of this report are described in the following.

Theory

The basic principles of sound transmission is treated, as well as the transfer matrix method and spatially windowing technique. Some methods of modelling energy losses is investigated, and the basics of SEA modelling are reviewed.

The model

Based on the theory, a SEA model that uses the transmission factor calculated with the transfer matrix method is presented.

Validation

SEA modelling is performed with the software AutoSEA v. 1.5 to validate and compare the results. Measurement data from references [1, 2] is also used to validate the result.

2 Basic principles of sound transmission

In this section, some characteristics of airborne sound transmission is presented for single and double walls. Impact sound is not considered.

The power transmission factor τ of a surface is defined as the ratio of the transmitted power W_t and the power incident on the surface W_i.

$$\tau = \frac{W_t}{W_i} \tag{1}$$

The sound reduction index (sometimes called transmission loss) is defined in dB as

$$R = 10 \log \frac{1}{\tau}. \tag{2}$$

With p denoting the pressure and v the particle velocity, the acoustical power is defined as

$$W = \frac{1}{2}\Re\{p^* v\} = \frac{|p|^2}{2}\Re\{1/Z_c\}, \tag{3}$$

where * denotes the complex conjugate, and Z_c the characteristic impedance of the medium, $Z_c = p/v$. The power transmission factor can therefore be written as

$$\tau = \left|\frac{p_t}{p_i}\right|^2 \tag{4}$$

provided that the medium is the same on the input and output side [3]. The power transmission factor can be seen as the ratio between the amplitude of the transmitted and incident wave.

Another way to approach the power transmission factor is to consider two rooms separated by a wall. Assume that the sound field in both rooms are diffuse. The sound intensity at the wall in the sending room is given by

$$W_i = \frac{\tilde{p}_S^2}{4\rho_0 c_0} S \tag{5}$$

where p_S denotes the sound pressure in the sending room and S the surface of the separating wall. The power transmitted through the wall is

$$W_t = \frac{\tilde{p}_R^2}{4\rho_0 c_0} A_R. \tag{6}$$

where $\tilde{p}_R$ and A_R denotes the pressure and total absorption area of the receiving room. Combining equation 5 and 6 gives an expression for the transmission factor,

$$\tau = \frac{\tilde{p}_R^2}{\tilde{p}_S^2}\frac{A_R}{S}. \tag{7}$$

And the sound reduction index

$$R = L_S - L_R + 10\log\frac{S}{A_R}. \tag{8}$$

The power transmission factor can therefore also be seen as the difference in sound pressure level with a correction due to absorption in the receiving room. [4]

2.1 Single wall

The general behaviour of sound transmission through a single panel is given. First, infinite panels are considered, then what happens when the panel is not of infinite extent.

2.1.1 Infinite panel

At low frequencies, the wavenumber in air is smaller than the plate wavenumber, $k_p > k_a$, and the wavelength in the plate is smaller than the wavelength in air. There is no angle at which an incidence wave can fit to the wavelength in the structure. This means no resonant transmission. The incidence wave will experience an obstacle with mass per unit area m''. This mass will be excited with a forced vibration. This type of transmission is called non-resonant transmission, or mass-law, and the transmission factor comes from the plate impedance $Z_p = j\omega m''$. The frequency where the wavelength in air is equal to the plate wavelength is called critical frequency. Above the critical frequency, where $k_p < k_a$, there will always be some angle at which the wavelength in the plate can match the wavelength in air. Thus, the plate will be excited with free vibrations. In this frequency region, just above the critical frequency, the transmission is fairly high but as the frequency goes up generally more and more of the vibrational energy in the plate are transformed into heat.

2.1.2 Finite panel

The edges of a finite panel give an increase in radiation efficiency in the frequency range below the critical frequency. This is illustrated in figure 1. In case (a) the wavelength in air is larger than the wavelength in the plate in both directions. If the plate would be infinite, no radiation would occur, the radiated wave field would consist of an acoustic short-circuit. But because of the finite size of the plate, the short-circuit is unsuccessful at the corners. Going up in frequency, the wavelength in one direction of the plate will be larger than the wavelength in air, leading to case (b). And above the critical frequency effective radiation will occur in the whole plate, case (c). [5]

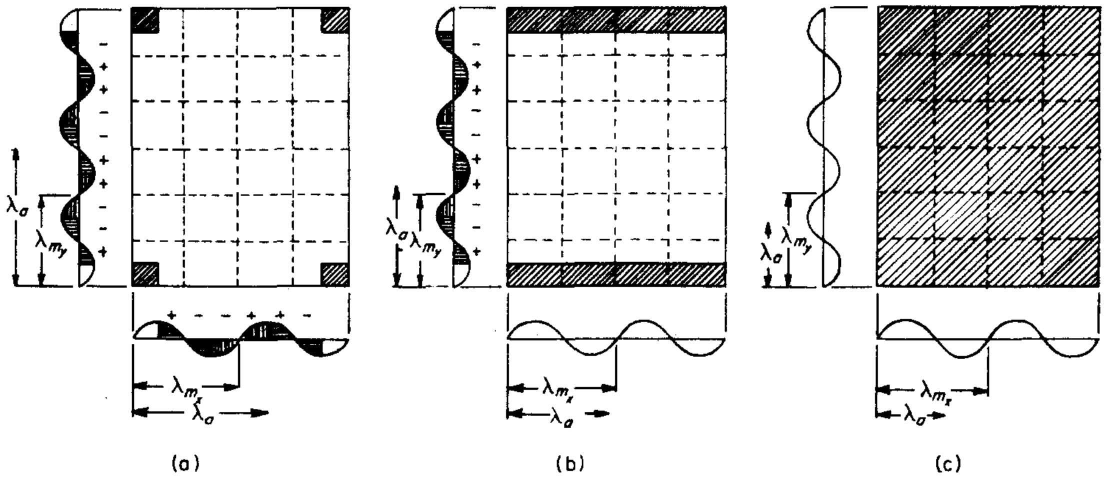

Figure 1: Wavelength relations and effective radiation area for corner, edge and surface modes. (a) corner mode; (b) edge mode; (c) surface mode. The dark area in the plates represents effective radiation. From [5].

But there are also other effects due to the finite size of the panel. The mode shapes of of the exited panel are of importance as well as the stiffness of the plate. At very low frequencies, the panel is stiffness controlled, leading to an increase in reduction index.

A generally accepted approximation of sound reduction index of a wall are [4]

$$R = \begin{cases} R_d - 10\log_{10}\left[\ln\left(\frac{2\pi f}{c_0}\sqrt{ab}\right)\right] + 20\log_{10}\left[1-\left(\frac{f}{f_c}\right)\right] + 5 \text{ dB}, & f < f_c \\ R_d + 10\log_{10}(2\eta\frac{f}{f_c}) \text{ dB}, & f > f_c \end{cases} \tag{9}$$

where $R_d = 20\log_{10}(m''f) - 47$ dB is the diffuse field mass-law. The mass-law gives an increase in reduction index of +6 dB/octave. The term containing the plate dimensions, a and b, takes the finite size of the plate into account. The term with the ratio of the frequency and critical frequency, f_c is close to zero at low frequencies. But as the frequency approaches the critical frequency, this term approaches $-\infty$, leading to a very poor reduction index at the critical frequency. Above the critical frequency the increase in reduction index is +9 dB/octave. The damping of the plate, η is significant in this frequency region.

The reduction index of a gypsum board with dimensions 3 m $\times$ 3 m $\times$ 10 mm is shown in figure 2. It is calculated with formulas given in SS-EN 12354-1 [6], which is somewhat more complicated than equation 9. Figure 2 clearly shows the slope of +6dB/octave in the mass law region, and the dip around the critical frequency. The material characteristics of the gypsum board is given in table 2, in section 8.

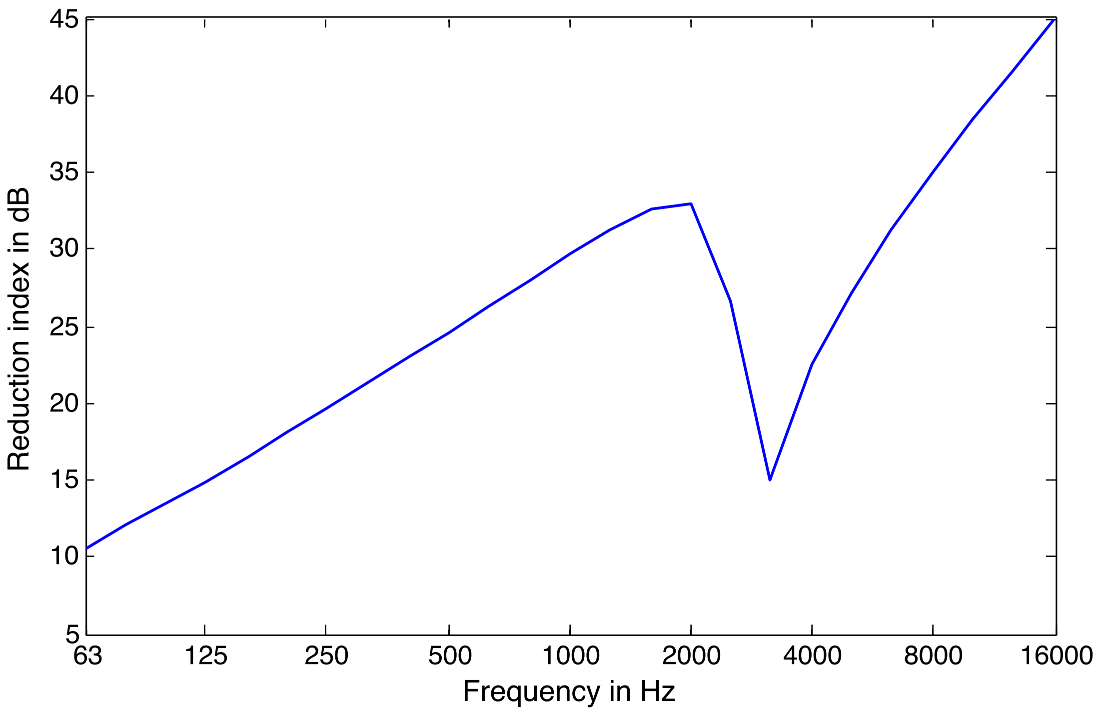

Figure 2: Sound reduction index of a single gypsum panel. Calculated with formulas in SS-EN 12354-1 [6].

2.2 Double wall

Consider a double wall consisting of two single panels with reduction indices R_1 and R_2 separated by an air cavity, without structural connections. Assume diffuse field in both rooms separated by the double wall, and also in the separating cavity. This is only valid for high frequencies, where the wavelength is much shorter than the depth of the cavity. In this case we can express the reduction indices, using equation 8 as

$$R_1 = L_S - L_C + 10\log\frac{S}{A_C} \tag{10}$$

$$R_2 = L_C - L_R + 10\log\frac{S}{A_R}. \tag{11}$$

where S denotes the separating surface and L and A the sound pressure level and total absorption area. The subscripts S, C and R represents the sending room, the cavity and the receiving room. The sound reduction index of the double wall is

$$R_{dw} = L_S - L_R + 10\log\frac{S}{A_R}. \tag{12}$$

Inserting equation 10 and 11 gives

$$R_{dw} = R_1 + R_2 + 10\log\frac{A_C}{S}. \tag{13}$$

This expression is valid for frequencies above $f_d \approx 55/d$. For a cavity depth of $d = 50$ mm this frequency is $f_d = 1100$ Hz. In this frequency range the reduction index of the double wall is dependent on the reduction indices of both single walls as well as the cavity damping.

For lower frequencies the double wall can be seen as a mass-spring system, the two leafs acts as masses coupled by the air cavity which acts as a spring. This system has a resonance at

$$f_0 = \frac{c_0}{2\pi}\sqrt{\frac{\rho_0(m_1'' + m_2'')}{m_1'' m_2'' d}}. \tag{14}$$

For a cavity filled with porous material the resonance frequency will be slightly different. [4] At this frequency, called the double wall resonance, there is a dip in reduction index. Below this frequency the two plates vibrate in phase with forced vibrations, the two plates acts as a single plate, having a mass equal to the sum of the masses of the plates.

Sharp (1978) presented the following empirical model for predicting the reduction index of double walls without structural connections, having the cavity filled with a porous absorber,

$$R = \begin{cases} R_M, & f < f_0 \\ R_1 + R_2 + 20\log_{10}(fd) - 29 \text{ dB}, & f_0 < f < f_d \\ R_1 + R_2 + 6 \text{ dB}, & f > f_d \end{cases} \tag{15}$$

Here, R_M is the reduction index of a panel with mass $M = m_1'' + m_2''$, R_1 the reduction index of the first panel and R_2 the reduction index of the second panel. [4]

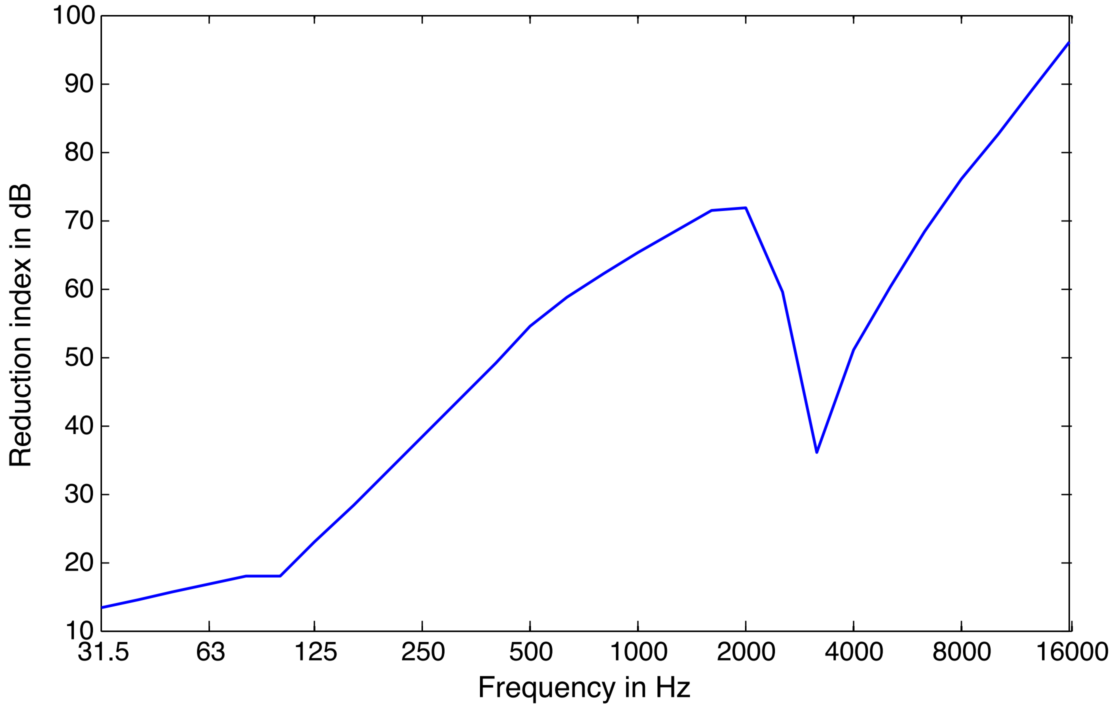

Figure 3: Sound reduction index of a double gypsum panel. Calculated with formulas in SS-EN 12354-1 [6] and the empirical model by Sharp, equation 15.

In figure 3, the reduction index of a double gypsum wall consisting of two identical gypsum boards with dimensions 3 m × 3 m × 10 mm is shown. The panels are separated by an air gap of 100 mm, and the material characteristics of the gypsum boards are given in table 2, in section 8.

The critical frequency of the boards and the double wall resonance of the system is indicated by a dip in reduction index, in figure 3. Below, the double wall resonance, the slope of the reduction index is about +6 dB/octave, and at about 500 Hz, there is a change in slope. This is due to the frequency f_d, which is $f_d \approx 550$ Hz for this double wall.

2.3 Diffuse field

The final expressions for reduction index of a single and double wall (equation 9 and equation 15) where determined empirically. The expressions are not for a certain incidence angle, but for the sum of all the incidence angles present. A diffuse field is often assumed in calculations. This means that the sound energy density is equal everywhere in the room, and the probability of sound coming from a certain angle is equal for all angles. In the next chapters, an incidence angle dependence is introduced for calculations of the transmission factor, i.e $\tau = \tau(\theta)$. To calculate the transmission loss for diffuse field excitation, the contribution from all angle is summed in an integral

$$\tau_d = \frac{\int_0^{\theta_{lim}} \tau(\theta) \cos\theta \sin\theta \, \mathrm{d}\theta}{\int_0^{\theta_{lim}} \cos\theta \sin\theta \, \mathrm{d}\theta}, \tag{16}$$

where $\theta_{lim} = 90°$. However, sometimes θ_{lim} is reduced to about 80° to get better agreement with measurements. [1]

3 Transfer matrix method

Figure 4 illustrates a plane wave impinging upon a material with thickness d, at an incidence angle θ. The material is infinite in x_1- and x_2-direction. The incoming wave give rise to a wave field in the finite medium, where the x_1-component of the wave number is equal to the x_1-component of the wave number in air, $k_a \sin\theta$, where k_a is the wave number in free air. Sound propagation in the layer is represented by a transfer matrix $[T]$ such that

$$\mathbf{V}(M) = [T]\mathbf{V}(M'), \tag{17}$$

where M and M' are the points in figure 4 and the components of the vector $\mathbf{V}(M)$ are the variables that describe the acoustic field at point M. Adopting

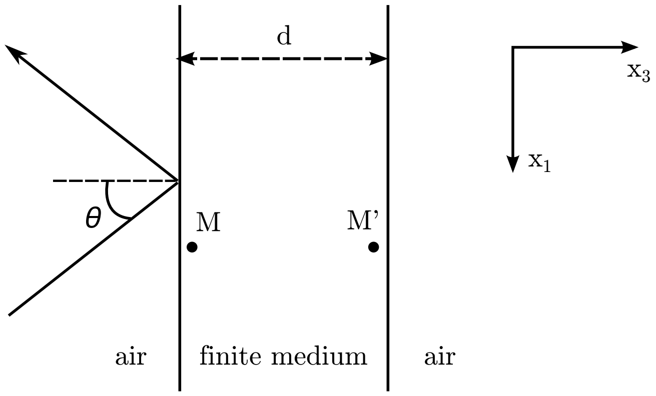

Figure 4: Plane wave impinging on a layer of thickness d, at incidence angle θ.

pressure p and particle velocity v as state variables, the relationship between the state variables each side of the layer can be written as

$$\begin{bmatrix} p(M) \\ v_3(M) \end{bmatrix} = \begin{bmatrix} T_{11} & T_{12} \\ T_{21} & T_{22} \end{bmatrix} \begin{bmatrix} p(M') \\ v_3(M') \end{bmatrix}. \tag{18}$$

Note that the x_3-component of the particle velocity is the state variable, i.e. the velocity normal to the layer surface. For isotropic and homogenous layer the following relations hold [7],

$$T_{11} = T_{22} \tag{19}$$

$$T_{11}T_{22} - T_{21}T_{12} = 1. \tag{20}$$

The latter of these two equations could also be stated as $\det(T) = 1$. Since it is not zero, this indicates that the transfer matrix is invertible. For a multilayered structure, the relationship between the state variables on the input and output side are obtained by multiplication of the transfer matrix of each layer. [3, 4, 8]

3.1 Thin elastic panel

Consider a thin elastic panel, e.g. a wall or plate with sound wave incident at an angle θ. The impedance of the panel, Z_p is defined as the ratio between the pressure difference across the panel and the velocity of the panel, $Z_p = (p_1 - p_2)/v_p$. By assuming that the normal velocity is equal on both sides of the layer $v_1 = v_2 = v_p$, the transfer matrix is written as

$$\begin{bmatrix} p_1 \\ v_1 \end{bmatrix} = \begin{bmatrix} 1 & Z_p \\ 0 & 1 \end{bmatrix} \begin{bmatrix} p_2 \\ v_2 \end{bmatrix}. \tag{21}$$

An expression for the impedance of the panel is given in [4] as

$$Z_p = \frac{B}{j\omega}(k_a^4 \sin^4\theta - k_p^4), \tag{22}$$

where B denotes the bending stiffness of the panel, k_a the wave number in air, k_p the wave number for bending waves in the panel, and θ the angle of incidence. Looking at equation 22 it is obvious that for $k_a > k_p$ there exists an incidence angle θ where Z_p is equal to zero, making the panel velocity infinitely large. By introducing some energy losses in terms of a complex bending stiffness $B(1 + j\eta)$ and also rewriting equation 22 in terms of the critical frequency f_c the impedance is given as

$$Z_p = j\omega m \left[1 - (1 + j\eta)\sin^4\theta \left(\frac{f}{f_c}\right)^2\right], \tag{23}$$

where m denotes mass per unit area of the panel. Equation 23 clearly shows the mass-law behaviour at low frequencies, well below the critical frequency. It is also shown that for normal incidence, $\theta = \pi/2$ the second term vanishes and only the mass impedance remains.

3.2 Fluid layer

For a sound wave with incidence angle θ into a fluid layer of thickness d, with wave number k and characteristic impedance Z_c, the pressure and velocity in x-direction is written as

$$p(x) = Ae^{-jk\cos\theta x} + Be^{jk\cos\theta x} \tag{24}$$

$$v_x(x) = \frac{\cos\theta}{Z_c}\left(Ae^{-jk\cos\theta x} - Be^{jk\cos\theta x}\right), \tag{25}$$

where A and B are amplitudes determined by boundary conditions. On the left boundary of the fluid layer, where $x = 0$ the pressure and velocity are

$$p_1 = p(0) = A + B \tag{26}$$

$$v_1 = v_x(0) = \frac{\cos\theta}{Z_c}(A - B). \tag{27}$$

Correspondingly, on the right-hand side, where $x = d$ the pressure and velocity are

$$p_2 = p(d) = (A + B)\cos(kd\cos\theta) - j(A - B)\sin(kd\cos\theta) \tag{28}$$

$$v_2 = v_x(d) = \frac{\cos\theta}{Z_c}\left((A - B)\cos(kd\cos\theta) - j(A + B)\sin(kd\cos\theta)\right). \tag{29}$$

Insertion of equation 26 into equation 28 and equation 27 into equation 29 yields

$$p_2 = \cos(kd\cos\theta)p_1 - j\frac{Z_c\sin(kd\cos\theta)}{\cos\theta}v_1 \tag{30}$$

$$v_2 = \cos(kd\cos\theta)v_1 - j\frac{\cos\theta\sin(kd\cos\theta)}{Z_c}p_1. \tag{31}$$

Putting equation 30 and equation 31 in matrix form and inverting gives the transfer matrix as

$$\begin{bmatrix} p_1 \\ v_1 \end{bmatrix} = \begin{bmatrix} \cos(kd\cos\theta) & j\dfrac{Z_c\sin(kd\cos\theta)}{\cos\theta} \\ j\dfrac{\sin(kd\cos\theta)}{Z_c}\cos\theta & \cos(kd\cos\theta) \end{bmatrix} \begin{bmatrix} p_2 \\ v_2 \end{bmatrix}. \tag{32}$$

In order to be consistent with other literature the wave number is substituted by the propagation coefficient $\Gamma = jk$ [4],

$$\begin{bmatrix} p_1 \\ v_1 \end{bmatrix} = \begin{bmatrix} \cosh(\Gamma d\cos\theta) & \dfrac{Z_c \sinh(\Gamma d\cos\theta)}{\cos\theta} \\ \dfrac{\sinh(\Gamma d\cos\theta)}{Z_c}\cos\theta & \cosh(\Gamma d\cos\theta) \end{bmatrix} \begin{bmatrix} p_2 \\ v_2 \end{bmatrix}. \tag{33}$$

As for the thin elastic panel, where energy losses were included as an complex bending stiffness, losses can be included in terms of a power attenuation coefficient, γ. This yields a complex propagation coefficient as $\Gamma = \gamma/2 + jk$, which is discussed in more detail in section 5.

3.3 Porous layer

A porous material is seen as a frame permeated by a network of pores filled with a fluid. For an elastic frame a model that takes motion of the frame and its coupling to the surrounding media into account is needed. Such a model is provided by the Biot theory. To model the acoustical field in a poroelastic layer, six variables instead of two are needed to describe the acoustical field in a fluid. This includes two velocity components of the frame, one velocity component of the fluid, two components of the stress tensor of the frame, and one in the fluid. [8]

If the frame of the porous layer can be seen as motionless, without displacement and deformation, a more simple model for the porous layer can be used. This situation occurs under acoustic excitations when the frame is heavy, constrained and rigid. It can also occur for an elastic frame when the solid-fluid coupling is negligible [9]. The porous layer is then modelled as an equivalent fluid, leading to a transfer matrix similar to the transfer matrix of a fluid layer. The losses are taken into account by a flow resistivity, r, from which a complex propagation coefficient and a complex characteristic impedance are calculated. [4] This is discussed further in section 5.

3.4 Interface to or from porous layer

As mentioned above, a porous layer is seen as a frame filled with the surrounding fluid. If this is air, the porosity σ is defined as the ratio of air volume to the total volume of the porous material, $\sigma = V_a/V_{tot}$. At the interface of a porous layer with porosity σ the pressure and volume flow is continuous. If the pressure and the velocity at the air side, $x = 0^-$ are denoted p_1 and v_1, and at the porous side, $x = 0^+$ are denoted p_2 and v_2, the continuity can be stated as

$$p_1 = p_2 \tag{34}$$
$$v_1 S = v_2 \sigma S, \tag{35}$$

where S denotes the cross section area of the interface. Writing this in matrix form yields the transfer matrix of the interface into a porous layer.

$$\mathbf{T_{to\,poro}} = \begin{bmatrix} 1 & 0 \\ 0 & \sigma \end{bmatrix}. \tag{36}$$

The transfer matrix of the opposite case, from a porous layer is the inverse, $\mathbf{T_{from\,poro}} = \mathbf{T_{to\,poro}}^{-1}$. Values of porosity typically lies very close to 1 [8].

3.5 The total transfer matrix

As a summary, the transfer matrices of different elements are given. The transfer matrix of a panel is taken from equation 21,

$$\mathbf{T_{panel}} = \begin{bmatrix} 1 & Z_p \\ 0 & 1 \end{bmatrix}. \tag{37}$$

Similarly, the transfer matrix of a fluid layer is take from equation 33,

$$\mathbf{T_{fluid}} = \begin{bmatrix} \cosh(\Gamma d \cos\theta) & \dfrac{Z_c \sinh(\Gamma d \cos\theta)}{\cos\theta} \\ \dfrac{\sinh(\Gamma d \cos\theta)}{Z_c} \cos\theta & \cosh(\Gamma d \cos\theta) \end{bmatrix}. \tag{38}$$

The transfer matrix of a porous layer with porosity σ is obtained as $\mathbf{T_{porous}} = \mathbf{T_{to\,poro}} \cdot \mathbf{T_{fluid}} \cdot \mathbf{T_{from\,poro}}$, where $\mathbf{T_{fluid}}$ is the matrix in equation 38. This gives the transfer matrix as

$$\mathbf{T_{porous}} = \begin{bmatrix} \cosh(\Gamma d \cos\theta) & \dfrac{Z_c \sinh(\Gamma d \cos\theta)}{\sigma \cos\theta} \\ \dfrac{\sinh(\Gamma d \cos\theta)}{Z_c} \sigma \cos\theta & \cosh(\Gamma d \cos\theta) \end{bmatrix}. \tag{39}$$

For example, the transfer matrix of a double wall consisting of two panels with an air gap in between is obtained by multiplying the transfer matrix of each element.

$$\mathbf{T_{dw}} = \mathbf{T_{panel,1}} \cdot \mathbf{T_{fluid}} \cdot \mathbf{T_{panel,2}} \tag{40}$$

3.6 Transmission factor from transfer matrix

The transmission factor of a structure is defined as the ratio of the transmitted power and the incident power. Sound power can be written as $W = \frac{1}{2}\Re\{p^*v\}$. With $Z_c = p/v$ the power is written as

$$W = \frac{1}{2}\Re\left\{\frac{p^*p}{Z_c}\right\} = \frac{|p|^2}{2}\Re\{1/Z_c\}. \tag{41}$$

Insertion of equation 41 in the definition of transmission factor yields

$$\tau = \frac{|p_t|^2}{|p_i|^2}\frac{\Re\{1/Z_{c,2}\}}{\Re\{1/Z_{c,1}\}}, \tag{42}$$

where $Z_{c,1}$ represents the characteristic impedance on the input side and $Z_{c,2}$ the characteristic impedance on the output side. This is illustrated in figure 5, where T denotes the transfer matrix of the structure considered,

$$\begin{bmatrix} p_1 \\ v_1 \end{bmatrix} = \begin{bmatrix} T_{11} & T_{12} \\ T_{21} & T_{22} \end{bmatrix} \begin{bmatrix} p_2 \\ v_2 \end{bmatrix}. \tag{43}$$

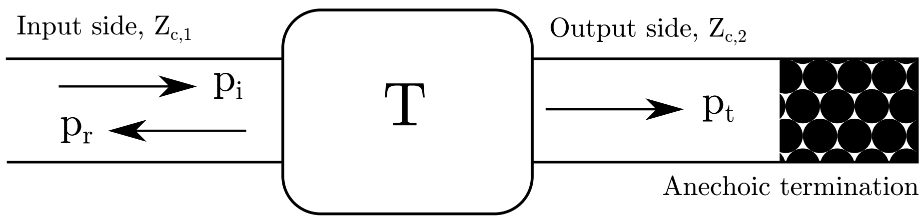

Figure 5: A system with transfer matrix T, with pressure field $p_i + p_r$ on the input side, and p_t on the output side.

The pressure and velocity on the input side is written as

$$p_1 = p_i + p_r \tag{44}$$

$$v_1 = (p_i - p_r)/Z_{c,1} \tag{45}$$

and the pressure and velocity on the output side is written as

$$p_2 = p_t \tag{46}$$

$$v_2 = p_t / Z_{c,2}. \tag{47}$$

Combining equation 44 and 45 gives

$$p_i = \frac{p_1 + v_1 Z_{c,1}}{2}. \tag{48}$$

Insertion of equation 43 yields

$$p_i = \frac{T_{11}p_2 + T_{12}v_2 + Z_{c,1}(T_{21}p_2 + T_{22}v_2)}{2}. \tag{49}$$

With expressions for pressure and velocity on the output side equation 49 becomes

$$p_i = \frac{1}{2}\left[T_{11}p_t + \frac{T_{12}p_t}{Z_{c,2}} + Z_{c,1}T_{21}p_t + \frac{Z_{c,1}T_{22}p_t}{Z_{c,2}}\right]. \tag{50}$$

Now we can express the ratio of the transmitted and incident pressure wave, which gives an expression for the transmission factor as

$$\tau = \frac{\Re\{1/Z_{c,2}\}}{\Re\{1/Z_{c,1}\}} 4 \left| T_{11} + \frac{T_{12}}{Z_{c,2}} + Z_{c,1}T_{21} + \frac{Z_{c,1}T_{22}}{Z_{c,2}} \right|^{-2}. \tag{51}$$

If the surrounding medium is the same on both the input and output side of the structure, the expression for transmission factor simplifies to

$$\tau = 4 \left| T_{11} + \frac{T_{12}}{Z_c} + Z_{c,1}T_{21} + T_{22} \right|^{-2}. \tag{52}$$

For an oblique incident wave, the transmission factor is instead written as [10]

$$\tau = 4 \left| T_{11} + \frac{T_{12}}{Z_c}\cos\theta + \frac{Z_{c,1}T_{21}}{\cos\theta} + T_{22} \right|^{-2}. \tag{53}$$

4 Spatial windowing technique

By means of transfer matrices it is possible to predict the transmission factor of a multilayered structure. This is however a prediction for a structure of infinite size. To take the finite size of the structure into account the spatial windowing technique, presented by Villot et al. [1] can be used.

4.1 Principle of the method

The method consists of spatial windowing of the pressure field on the input side of the structure, calculation of the resulting velocity field of the infinite structure and spatial windowing of the velocity field before calculating the radiated field on the output side of the structure.

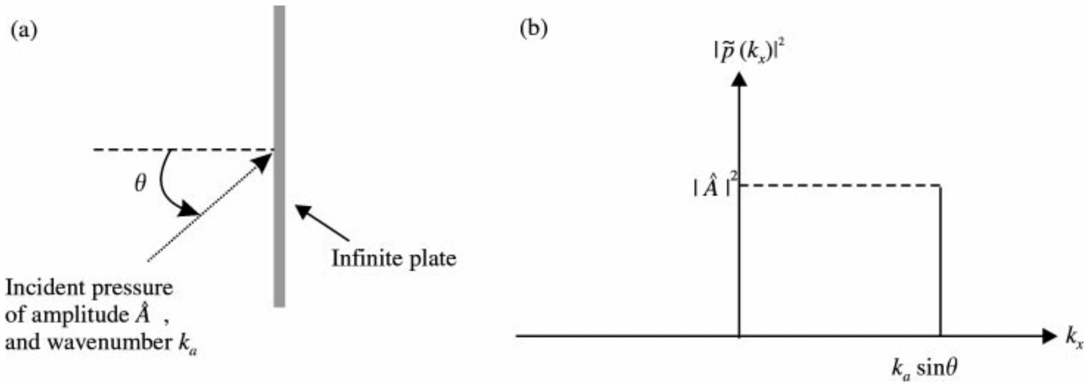

Figure 6: (a) Acoustically excited infinite plate and (b) associated incident pressure wavenumber spectrum. From [1].

Figure 6 shows an infinite plate, acoustically excited by a pressure wave with incidence angle θ, amplitude $\hat{A}$ and wavenumber k_a. The associated incident pressure wavenumber spectrum is also depicted, which is represented by the Dirac delta function at $k_x = k_a \sin(\theta)$. A single wavenumber $k_p = k_a \sin(\theta)$ will propagate in the structure. For low frequencies, below the critical frequency, the wavenumber in air is smaller than the plate wavenumber. This indicates that the plate cannot be excited, except for a forced wave, since there is no possibility to match the wavenumber in air with the plate wavenumber.

Applying a spatial window can be seen as if the incident pressure wave passes through a diaphragm before affecting the infinite structure as shown in figure

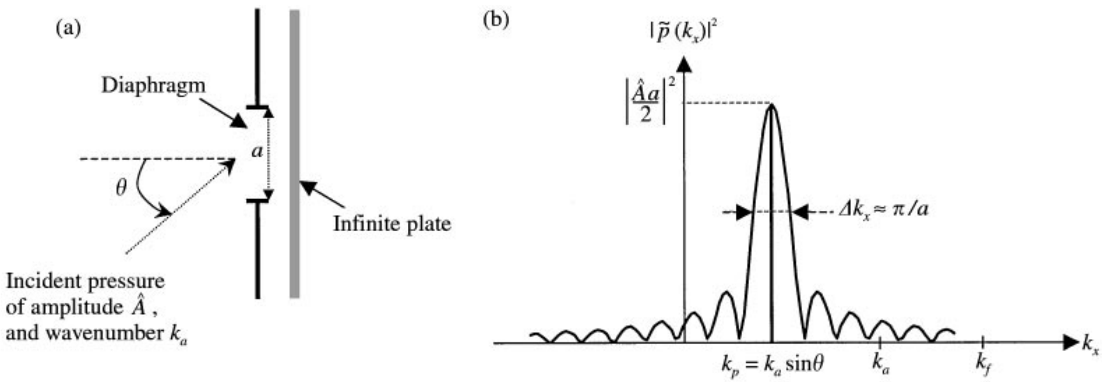

Figure 7: (a) Spatial windowing of acoustic incident field exciting an infinite plate and (b) associated incident pressure wavenumber spectrum. From [1].

7. The wavenumber spectrum will now be distributed over the entire wavenumber domain. This means that the plate can be excited even below the critical frequency with free waves. Similarly, a spatial window is applied on the radiated sound field.

The transmission factor for the finite structure is obtained by applying a spatial window as

$$\tau = \frac{\sigma}{\sigma_{inf}} \tau_{inf}, \tag{54}$$

where $\sigma_{inf} = 1/\cos(\theta)$ and σ the radiation efficiency associated with spatial windowing of the finite sized structure. If this i done twice it will result in

$$\tau(f,\theta) = \tau_{inf}(f,\theta)[\sigma(f,\theta)\cos(\theta)]^2. \tag{55}$$

4.2 Radiation efficiency

Villot et al. [1] gives an expression for the radiation efficiency as a double integral dependent of wavenumber in air, incidence angle and wave propagation angle in the plate. Since the influence of wave propagation angle is slight, a spatially averaged radiation efficiency over the plate is also given. This means no dependence of propagation angle in the plate, but instead a triple integral, which leads to very heavy calculations. A triple integral to be numerically evaluated for each frequency and each angle.

Vigran [2] gives a simplified version of the spatial window technique. Instead of plate dimensions a and b he uses one dimension $L = \sqrt{ab}$, this gives a much simpler expression for radiation efficiency as

$$\sigma(k_p) = \frac{Lk_a}{2\pi} \int_0^{k_a} \frac{\sin^2\left[(k_r - k_p)\frac{L}{2}\right]}{\left[(k_r - k_p)\frac{L}{2}\right]^2 \sqrt{k_a^2 - k_r^2}} \, \mathrm{d}k_r. \tag{56}$$

As before, k_a denotes the wavenumber in air and k_p the plate wavenumber. This simplification can be made when the aspect ratio of the object is less than 1:2.

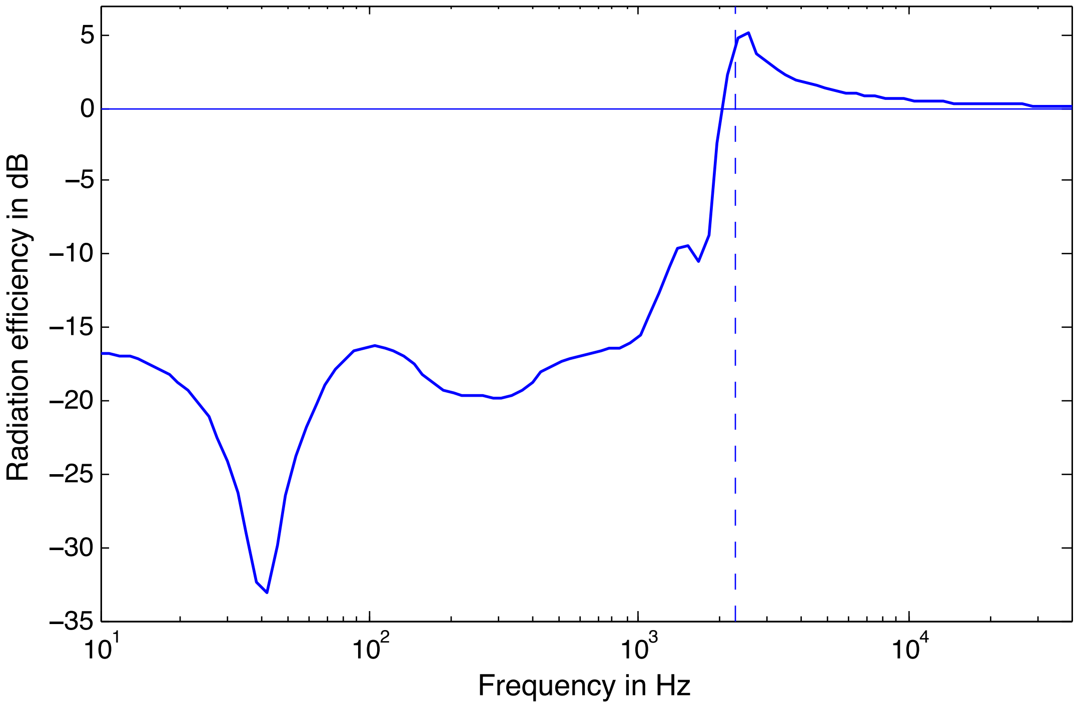

Figure 8: The radiation efficiency $\sigma(k_p)$ of a 15 mm gypsum board calculated with equation 56. The dashed line indicates the critical frequency, $f_c = 2.26$ kHz.

The radiation efficiency is calculated with insertion of the plate wavenumber for bending waves

$$k_p = \left(\frac{\omega^2 m'' 12(1-\nu^2)}{Et^3}\right)^{1/4} \tag{57}$$

in equation 56, were m'' is the mass per unit area of the plate, E Young's modulus and ν Poisson's ratio of the material. Figure 8 shows the radiation efficiency of a 1.4 m $\times$ 1.1 m $\times$ 15 mm gypsum board without internal damping, see table 2 in section 8 for material data. Above the critical frequency, the radiation efficiency behaves as the case of an infinite plate, with radiation efficiency approaching 1, or 0 dB. Below the critical frequency however, the radiation efficiency is not zero. This is an effect from the finite size of the plate.

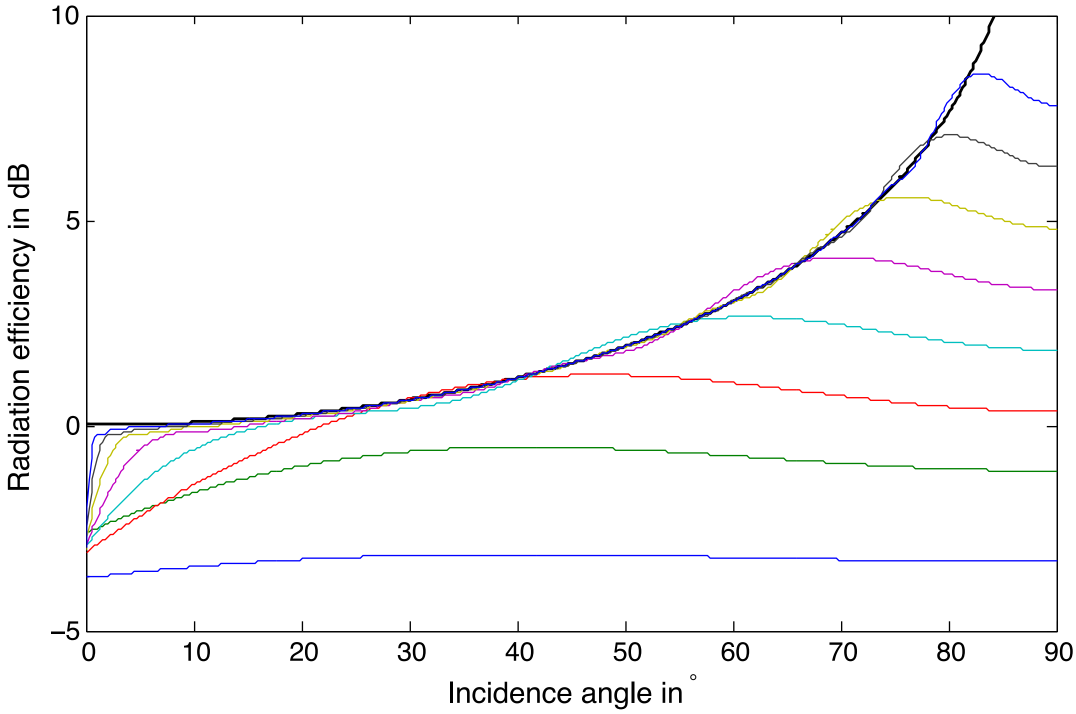

Figure 9: The radiation efficiency $\sigma(k_a \sin(\theta))$ calculated with equation 56. The black line represents the infinite case, $\sigma(k_a \sin(\theta)) = 1/\cos(\theta)$. The coloured lines from lowest to highest represents a spatial window of $k_aL = 2$, $k_aL = 4$, $k_aL = 8$, $k_aL = 16$, $k_aL = 32$, $k_aL = 64$, $k_aL = 128$, $k_aL = 256$.

The diffuse field radiation efficiency $\sigma(k_p = k_a \sin(\theta))$ is also calculated, which is not dependent of the material of the structure, but only the dimensions of the plate. Figure 9 shows the diffuse field radiation efficiency, for different values of k_aL. Small values of k_aL, indicates small dimensions, at least in comparison with the wavelength. For larger values of k_aL the radiation efficiency approaches the infinite case.

There is a dip of about 3 dB at small angles for all k_aL. This is probably due to the simplification of the formula for radiation efficiency, but Vigran states that the accuracy in the end result may in practice be maintained by this simplified procedure [2].

By looking at figure 9 it is seen that applying a spatial window with radiation efficiency as in figure 9 diminishes the contribution from angles close to grazing incidence to the diffuse field transmission factor. A similar effect is obtained by reducing the incident field diffuseness, which is a frequently used trick to obtain better agreement with measurement data, i.e. choose an upper limit $\theta_{lim} < 90°$ in the integral in equation 96.

4.3 Variations of the spatial windowing technique

There are several different versions of the spatial windowing technique. Villot et al. [1] states that the spatial window should be applied twice, whereas Vigran [2], who presents a simplified version of the spatial windowing technique, states that better agreement with measured result is obtained with a single spatial window. A similar approach is the finite transfer matrix method. And as mentioned in the previous section, the same type of result is obtained by reducing the diffusiveness of the incidence sound field.

4.3.1 Finite transfer matrix method

Allard and Atalla [8] give an extension to the transfer matrix method, called finite transfer matrix method (FTMM), which takes the finite size of the structure into account, similar to the spatial windowing technique. The radiation efficiency is calculated differently, but gives similar results as the spatial windowing technique [8]. In the FTMM a single correction is used, i.e. a single spatial window. Allard and Atalla states that using a double spatial window in the calculations of the transmission factor is in contradiction to the definition of the transmission coefficient. They recommend that the correction should be applied to the transmitted power only. But they also state that a correction may still be necessary to account for the diffusiveness of the incident field.

4.3.2 Reducing diffusiveness

As stated above, the diffusiveness of the incident sound field is often reduced from 90° to about 80° in order to get a better agreement with measurement data. However, this has also a physical explanation. Figure 10 shows the angles of incidence of all the modes in a 1/3 octave band as a function of incidence angle.

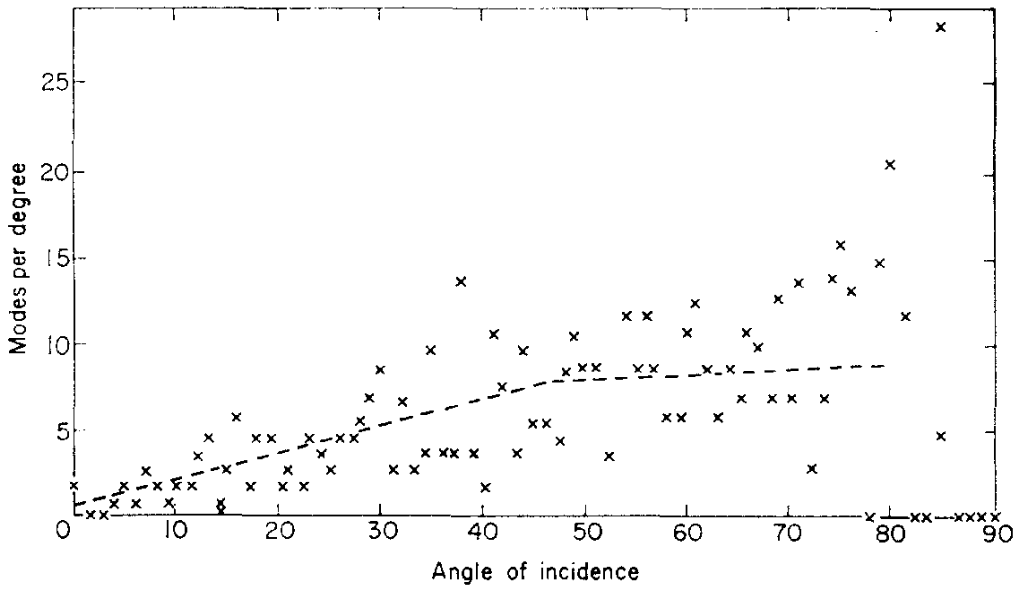

Figure 10: Scatter plot of modal density and incidence angle. From [11].

The number of modes increases gradually with incidence angle, and then falls sharply, with no incident sound above 84° [11].

As can be seen in section 8, predicted result of double walls reduction index is lower than measured values in the frequency range above the double wall resonance and below the critical frequency. The reason for this is that in diffuse field, in this frequency range, there will always be some angle for which the reduction index is zero (without damping included), and thus a low diffuse field reduction index. [11]

4.3.3 Adding resistance term to panel impedance

Another approach to obtain better agreement with measured values of reduction index of double panels is to add a resistance term R to the impedance of the individual panels

$$Z_p = \frac{2R}{\cos\theta} + j\omega m \left[1 - \sin^4\theta \left(\frac{f}{f_c} \right)^2 \right]. \tag{58}$$

This leads to a real part of the plate impedance that represents energy losses in the plates. Comparing with equation 23 it is obvious that the same type of behaviour is obtained by a complex bending stiffness, with the imaginary part of the bending stiffness, η representing the energy losses.

In this approach the resistance is divided by $\cos\theta$, leading to a real part that approaches infinity for angles close to grazing incidence. This provides a reduction of the contribution of transmission for high angles, which gives better agreement with measurements. However, the resistance term appears to have no physical explanation. [11]

5 Modelling energy losses

Any real vibration object experiences energy losses, e.g. vibrational energy is converted into heat. Some common methods for including energy losses are given in this section. In SEA modelling, the term loss factor is used.

5.1 Losses in structures

The most common approach for including energy losses in a structure, such as a plate, is to introduce a complex bending stiffness, with imaginary part η. This gives a real or dissipative part of the panel impedance, see equation 23. [12]

5.2 Losses in fluids

In fluids, energy losses can be taken into account by adding an imaginary part to the wave number,

$$k = \frac{\omega}{c}\left(1 - \frac{\eta}{2}\right). \tag{59}$$

Remembering that the propagation coefficient is jk, this corresponds to adding a real part, resulting in a complex propagation coefficient

$$\Gamma = j\frac{\omega}{c} + \frac{\omega\eta}{2c}. \tag{60}$$

Another common approach to take losses into account by a complex propagation coefficient is by adding a real part $\gamma/2$, where γ is called power attenuation coefficient. This gives pressure, exponentially decreasing with distance,

$$p(x) = \hat{p}\,\mathrm{e}^{-\Gamma x} \tag{61}$$

$$= \hat{p}\,\mathrm{e}^{-\gamma x/2}\,\mathrm{e}^{-j\omega x/c} \tag{62}$$

$$= p_0\,\mathrm{e}^{-\gamma x/2}, \tag{63}$$

where $p_0 = \hat{p}\,\mathrm{e}^{-j\omega x/c}$ is the pressure without energy losses. Since energy is proportional to the pressure squared, the energy will decrease exponentially,

$$E \sim p^2 \Rightarrow E = E_0\,\mathrm{e}^{-\gamma x}. \tag{64}$$

Hence the name power attenuation coefficient. The energy attenuation in dB per metre is approximately

$$\Delta L_w = 10\log_{10}(\mathrm{e}^{-\gamma}) \approx -4.3\,\gamma \text{ dB/m} \tag{65}$$

Comparing the two approaches of including losses gives a relation between the loss factor and power attenuation coefficient as [13]

$$\eta = \frac{c}{\omega}\gamma. \tag{66}$$

A different approach to include losses in wave propagation is to add a viscous loss term in the governing equation relating pressure and particle velocity

$$\frac{\partial p}{\partial x} = -\rho_0 \frac{\partial v_x}{\partial t} + r v_x, \tag{67}$$

where r is the airflow resistivity having dimension $\mathrm{Pa} \cdot \mathrm{s/m}^2$. This results in a complex propagation coefficient and a complex characteristic impedance,

$$\Gamma = j\frac{\omega}{c}\sqrt{1 - j\frac{r}{\rho_0 \omega}} \tag{68}$$

$$Z_c = \rho_0 c_0 \sqrt{1 - j\frac{r}{\rho_0 \omega}}. \tag{69}$$

Viscous losses are significant in porous materials. This is the simplest model for a porous material, a so-called Rayleigh model.

How large attenuation in dB per metre is the energy attenuation of propagation in a material with flow resistivity r? Remember that the energy attenuation for a wave with propagation coefficient Γ is

$$\Delta L_w = 10 \log_{10}(\mathrm{e}^{-\Re\{2\Gamma\}}). \tag{70}$$

The square root in the expression for the propagation coefficient complicates the calculation. But using the following approximations

$$\sqrt{1 - jx} \approx \begin{cases} 1 - jx/2, & \text{for } x << 1 \\ (1-j)\sqrt{x/2}, & \text{for } x >> 1, \end{cases} \tag{71}$$

where $x << 1$ corresponds to high frequencies and/or low flow resistivity and vice versa for $x >> 1$, the attenuation in dB/m is estimated to

$$\Delta L_w \approx \begin{cases} -0.0106\, r, & \text{for } \omega >> r \\ 10 \log_{10}(\mathrm{e}^{-0.038\sqrt{\omega r}}), & \text{for } \omega << r. \end{cases} \tag{72}$$

The expression for $\omega << r$ is not very clear, but because of the square root, the dependence is not linear so it can not be expressed as easy as for $\omega >> r$. For $r = 10000\ \mathrm{Pa \cdot s/m^2}$, which is a common value for mineral wool, the attenuation is around -40 dB/m at 100 Hz. [4]

There are also several empirical models for porous materials. A model by Delany and Bazley is often used due to its simplicity. They give purely empirical expressions for the complex propagation coefficient and the characteristic impedance, based on measurements on a wide range of materials having porosity of approximately one. The expressions are

$$\Gamma = j\frac{\omega}{c_0}[1 + 0.0978\, E^{-0.700} - j \cdot 0.189\, E^{-0.595}] \tag{73}$$

$$Z_c = \rho_0 c_0[1 + E^{-0.754} - j \cdot 0.087\, E^{-0.732}], \tag{74}$$

where $E = \rho_0 f / r$. It is assumed that E lies inside the range $0.01 - 1.0$, which indicates that the model works best for materials with high flow resistivity. [4]

6 SEA modelling

In this section, the basic principle of statistical energy analysis is summarised. Two important concepts in SEA, modal density and modal overlap factor, are explained and the applicability of SEA is discussed. An SEA model of two rooms separated by a common wall is given as an example. A system containing a double wall is also given as an SEA model, as well as the SEA model of two rooms separated by any element with known transmission factor. The damping loss factor and coupling loss factor of some common subsystem are also given.

6.1 Principles of SEA

Statistical energy analysis is a method for high frequency modelling, where finite element modelling is not applicable. It is applicable to structures that can be divided into subsystems coupled together, and it predicts the average sound and vibration levels, time and frequency averages as well as averages within each subsystem.

In SEA modelling the system is divided into subsystems and a power balance for each subsystem is set up based on the conservation of energy. The power flowing from one subsystem to another is assumed to be proportional to the difference in their modal energies, or energy per mode. This is in analogy with heat transfer; Energy flows from a hot subsystem to a colder until the temperature difference is zero. In SEA, vibrational energy per mode represents temperature. If the energy per mode is equal in two subsystems, the energy flow between them is zero. This assumption is called coupling power proportionality.

The power flow is assumed to be proportional to the damping. The dissipated energy from subsystem i is given by its damping loss factor (DLF) η_{id},

$$W_{id} = \omega \eta_{id} E_i, \tag{75}$$

where E_i denotes the energy in subsystem i. Similarly, the power flowing from subsystem i to subsystem j is proportional to the coupling loss factor (CLF), η_{ij} as

$$W_{ij} = \omega \eta_{ij} E_i. \tag{76}$$

The coupling power proportionality implies that the coupling loss factors satisfy the so called consistency relation

$$n_i \eta_{ij} = n_j \eta_{ji}, \tag{77}$$

where n is the modal density, i.e. the number of modes per frequency.

6.2 Modal density and modal overlap factor

A standing wave pattern is caused by constructive interference. The amplitude of the wave increases until the energy lost by damping is equals the power input to the system. This standing wave pattern is called a mode (or resonance). An assumption made in SEA is that the response of the subsystem is due to these resonances and that other motion can be ignored. A result of this assumption is that the response of a subsystem is directly proportional to the damping. [13]

Another assumption made in SEA is that there are enough resonances in a frequency band for individual modes to be unimportant. The number of modes that lies in an increment of frequency is called modal density, $n(f)$. The expressions for modal density of some common subsystems are given in table 1, but the derivation is not described. For a room (3D cavity), V denotes the volume of the room, S' the total surface area and P' the the total length of all edges. For a plate and a 2D cavity, i.e. a room with one dimension to small for any wave motion in that direction, S denotes the surface area.

Table 1: The modal density, $n(f)$ in modes/Hz, of some common subsystems. [13]

Subsystem	3D cavity	2D cavity	plate in bending
$n(f)$	$\frac{4\pi f^2 V}{c_0^3} + \frac{\pi f S'}{2c_0^2} + \frac{P'}{8c_0}$	$\frac{2\pi f S}{c_0^2}$	$\frac{\pi S f_c}{c_0^2}$

A main assumptions in statistical energy analysis is that the response is determined by resonant modes. The analysis is valid when there are many modes present in every subsystem. If there is a insufficient number of modes in a subsystem the estimation of coupling loss factor may have large errors. This condition results in a lower frequency limit where statistical energy analysis is appropriate. But the limit is quite fluent, there is usually a gradual increase in the error with decreasing frequency. Suggested minimum number of modes in a frequency band necessary for statistical averaging lies between 2 and 30 modes per frequency band. But the consideration of number of modes alone is insufficient in order to determine the lower limit of SEA. [13]

The damping of the resonant modes is also important in SEA modelling. If the damping is high the frequency response of a subsystem will be smoother than if the damping were low. The modal overlap factor is defined as the ratio of the modal bandwidth to the average frequency spacing between modes. It is a more useful measure of the applicability of SEA, since it takes both the number of modes and the damping of these modes into account. A high number of modes gives a low frequency spacing between the modes, which results in a high modal overlap factor. High damping gives a wider resonance peak and thus larger bandwidth which results in a high modal overlap factor. [13]

Using half-power bandwidth the modal overlap factor, M is calculated as

$$M = f\eta n, \tag{78}$$

where η is the total loss factor and n the modal density of the subsystem. If the modal overlap factor i less than 1 a part of the frequency spectrum will not be damping controlled, which is assumed in SEA. [13] However, if the damping is too large the response is not determined by resonant modes, since the waves will be attenuated before reflections at the edges occur.

6.3 Single wall

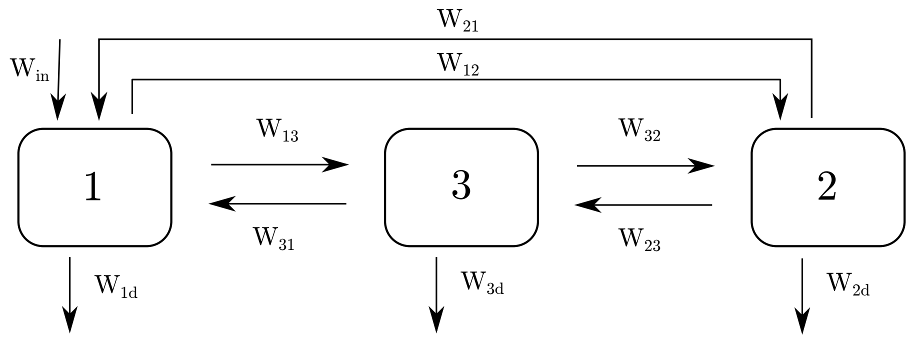

Figure 11: The SEA model of two rooms separated by a common wall.

As an example, the SEA model of two rooms separated by a common wall is considered. The SEA model of this system is shown in figure 11. The sending room, i.e. the room containing the source is modelled as subsystem 1, the receiving room subsystem 2 and the separating wall subsystem 3. Figure 11 illustrates the power flow to and from the subsystems. For subsystem i, W_{id} represents the dissipated power. Most often this is the energy that is transformed into heat. The power flowing between subsystem 1 and 3 is due to the coupling between the sending room and the wall, which mostly is important above the critical frequency of the wall. Similarly, the coupling of the wall and the receiving room, represented by W_{32} and W_{23} is important above the critical frequency. The direct coupling between the rooms represents the mass-law or forced transmission, (see further section 2.1). This is significant at low frequencies, but is sometimes negligible at high frequencies, in comparison with the resonant transmission. [13]

Writing the power balance for this system leads to three equations,

$$W_{in} + W_{21} + W_{31} = W_{1d} + W_{12} + W_{13} \tag{79}$$

$$W_{12} + W_{32} = W_{2d} + W_{21} + W_{23} \tag{80}$$

$$W_{13} + W_{23} = W_{3d} + W_{31} + W_{32}. \tag{81}$$

Expressing the power flow in terms of energy, $W = \omega\eta E$ and rewriting in matrix form gives

$$\begin{bmatrix} \eta_{1d} + \eta_{12} + \eta_{13} & -\eta_{21} & -\eta_{31} \\ -\eta_{12} & \eta_{2d} + \eta_{21} + \eta_{23} & -\eta_{32} \\ -\eta_{13} & -\eta_{23} & \eta_{3d} + \eta_{31} + \eta_{32} \end{bmatrix} \begin{bmatrix} E_1 \\ E_2 \\ E_3 \end{bmatrix} = \begin{bmatrix} W_{in}/\omega \\ 0 \\ 0 \end{bmatrix}. \tag{82}$$

Since the loss factor is a positive quantity, the matrix in equation 82 is positive definite and thus invertible. So if all the loss factors and the input power is known, the energy in all subsystems, E_1, E_2 and E_3 can easily be obtained.

It may be convenient to introduce a total loss factor, η_i which is the fraction of the total power leaving the subsystem i. In this case $\eta_1 = \eta_{1d} + \eta_{12} + \eta_{13}$ is the total loss factor for subsystem 1, $\eta_2 = \eta_{2d} + \eta_{21} + \eta_{23}$ is the total loss factor of subsystem 2 and $\eta_3 = \eta_{3d} + \eta_{31} + \eta_{32}$ is the total loss factor of subsystem 3.

Equation 82 may then be rewritten as

$$\begin{bmatrix} \eta_1 & -\eta_{21} & -\eta_{31} \\ -\eta_{12} & \eta_2 & -\eta_{31} \\ -\eta_{13} & -\eta_{23} & \eta_3 \end{bmatrix} \begin{bmatrix} E_1 \\ E_2 \\ E_3 \end{bmatrix} = \begin{bmatrix} W_{in}/\omega \\ 0 \\ 0 \end{bmatrix}. \tag{83}$$

6.4 Double wall

If the two rooms instead are separated by a double wall, i.e. two panels separated by a cavity, possibly filled with absorbing material. The SEA model now contains five subsystems, as illustrated in figure 12. A non-resonant transmission path between subsystem 1 and 2 could also be included. But this type of transmission only occurs below the double wall resonance, see section 2.2. This resonance typically lies below 100 Hz, a frequency where SEA modelling possibly is not very appropriate.

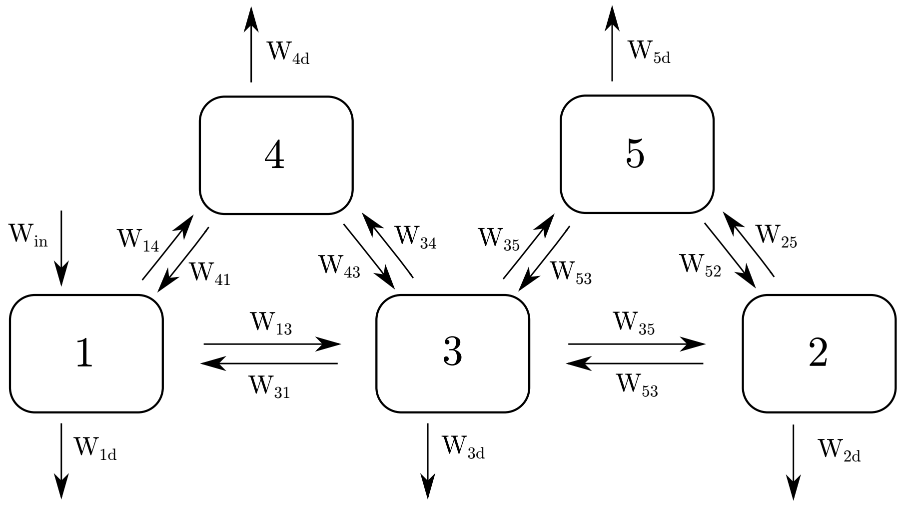

Figure 12: The SEA model of two rooms separated by a common double wall.

6.5 Total and damping loss factor

A common measure for damping in a room (3 dimensional cavity) is the reverberation time, T_{60}, which is the time for the energy to decay 60 dB once a steady source has been turned off. The total loss factor and reverberation time are related as

$$\eta = \frac{2.2}{fT_{60}} \tag{84}$$

In a cavity, where one dimension is too small for any wave motion to occur (2 dimensional cavity) the reverberation time is not convenient to characterise the damping. The cavity may be filled with a porous absorber. There are several methods for modelling the damping in a cavity, see section 5, but all methods lead to a complex propagation coefficient Γ. As described in section 5, the damping loss factor and complex propagation coefficient related as [4, 13]

$$\eta_d = \frac{2\Re\{\Gamma\}}{\Im\{\Gamma\}} \tag{85}$$

For panels, the damping loss factor is often stated together with other material characteristics.

6.6 Coupling loss factor

The coupling loss factor between a panel and a room is defined as the fraction of energy of the panel that is radiated into the room in one radian cycle. For a panel with area S vibrating with velocity v the radiated power is

$$W_{rad} = v^2 \rho_0 c_0 S \sigma, \tag{86}$$

where σ is the radiation factor of the panel. By definition, the power radiated from a panel, 1, to a room, 2, in SEA notation is

$$W_{12} = \eta_{12} \omega E_1 = \eta_{12} m'' S v^2 \omega. \tag{87}$$

Since the power flowing from the plate to the room is the same as the radiated power, combining these expressions gives

$$\eta_{12} = \frac{\rho_0 c_0 \sigma}{2\pi f m''}. \tag{88}$$

The coupling loss factor from a room to a panel is obtained with the consistency relation, $n_1 \eta_{12} = n_2 \eta_{21}$. [13]

The coupling loss factor between two rooms can be obtained if the transmission factor of the separating element is known. For a reverberant room, the power incident on a wall with area S is

$$W_i = \frac{Ec_0S}{4V}. \tag{89}$$

From the definition of transmission factor, the transmitted power is

$$W_t = \tau W_i = \frac{Ec_0S\tau}{4V}. \tag{90}$$

In SEA notation, the power transmitted between any rooms 1 and 2 is

$$W_{12} = \omega\eta_{12}E_1. \tag{91}$$

Combining these two expressions gives the coupling loss factor as

$$\eta_{12} = \frac{c_0L\tau_d}{8\pi fV_1}, \tag{92}$$

where τ_d is the transmission factor for diffuse field. This transmission factor is used since SEA assumes diffuse field in the rooms.

7 The model

In this section a model of two rooms separated by a multilayered wall is presented, using the theory from previous sections. The wall is modelled with transfer matrices. From the total transfer matrix the power transmission factor of the wall is calculated, which is plugged into the SEA model.

7.1 SEA formulation

Two rooms separated by a multilayer is the system considered. The SEA model of the system is shown in figure 13. The sending room is denoted subsystem 1 and the receiving room is denoted subsystem 2. The subsystems are defined by its dimensions $a \times b \times c$, where $S = a \times b$ is the surface area of the separating wall, and its total loss factor η_i. The coupling loss factors η_{ij} and η_{ji} are calculated from the power transmission factor with equation 92. Setting up the power balance equations and solving for energy as in section 6 gives the energy in subsystem 1 as

$$E_1 = \left[\frac{\eta_2}{\eta_1 \eta_2 - \eta_{12} \eta_{21}} \right] \frac{W_{in}}{\omega}, \tag{93}$$

and the energy in subsystem 2 as

$$E_2 = \frac{\eta_{12}}{\eta_2} E_1. \tag{94}$$

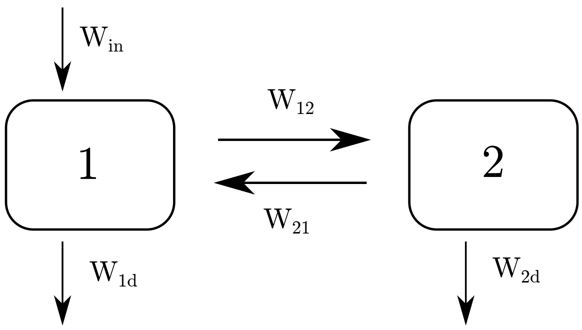

Figure 13: The implemented SEA model.

7.2 The transmission factor

The transmission coefficient is needed to estimate the coupling loss factors in the SEA model of the system. It is calculated from the total transfer matrix of the multilayered wall, which is calculated with equation 40 in the case of a double wall. The total transfer matrix is a function of incidence angle and frequency, $T_{tot} = T_{tot}(f,\theta)$. The power transmission factor, $\tau_{inf}(f,\theta)$ is calculated with equation 53. To take the finite size of the separating wall into account, a double spatial window is applied to the power transmission factor of the infinite system.

$$\tau(f,\theta) = \tau_{inf}(f,\theta)[\sigma(k_a \sin(\theta))\cos(\theta)]^2, \tag{95}$$

where $\sigma(k_a \sin\theta)$ is the radiation factor calculated with the simplified formula, equation 56.

Since the SEA model presented in the previous section assumes diffuse field in the subsystems, the power transmission factor for diffuse field is required to calculate the coupling loss factors. It is obtained by integration of the power transmission coefficient over all angles of incidence

$$\tau_d(f) = \frac{\int_0^{\theta_{lim}} \tau(f,\sigma)\cos(\theta)\sin(\theta)\ \mathrm{d}\theta}{\int_0^{\theta_{lim}} \cos(\theta)\sin(\theta)\ \mathrm{d}\theta} \tag{96}$$

where θ_{lim} is the selected diffuse field integration limit, usually 90° [8]. With the spatial windowing technique, there is no need to reduce the diffusiveness of the incidence sound field [1].

8 Validation

In this section, the model is compared to results from measurement data from Villot et al. [1] and Vigran [2] and with AutoSEA v. 1.5. Three different separating elements are considered, a single aluminium plate, a double glazing and a double gypsum wall. The material data are given in table 2.

Table 2: Material characteristics. From references [1, 14].

	Aluminium	Glass	Gypsum
Thickness	1.1 mm	4 mm	10 mm
Density	2700 kg/m^3	2500 kg/m^3	850 kg/m^3
Young's modulus	70.0 GPa	62.0 GPa	4.1 GPa
Poisson's ratio	0.33	0.22	0.3
Internal damping	0.01	0.05	0.01
Critical frequency	10.9 kHz	3.18 kHz	2.82 kHz

8.1 Single aluminium plate

8.1.1 Transmission factor

The transmission factor for an aluminium plate is calculated as in section 7. The transmission factor is calculated from the transfer matrix of the plate and spatially windowed with a window of dimension $L = \sqrt{1.4 \times 1.1}$ m. The material characteristics of the plate are shown in table 2. Figure 14 shows the reduction index of the aluminium plate. Measured values of the reduction index is taken from Villot et al. [1]. The red dash-dotted line represents an infinite system, i.e. not spatially windowed. It differs from the measured values of about -6 dB in the whole frequency range. For the red dotted line, the incident diffuse field is reduced from 90° to 78°. This gives better agreement with the measured data, but only for high frequencies. For the blue line, the system is spatially windowed with a double window, which seems to give good agreement with the measurement in the whole frequency range. The blue dashed line is also spatially windowed, but with a single window. It is suggested by Vigran [4] and Allard and Atalla [8] that a

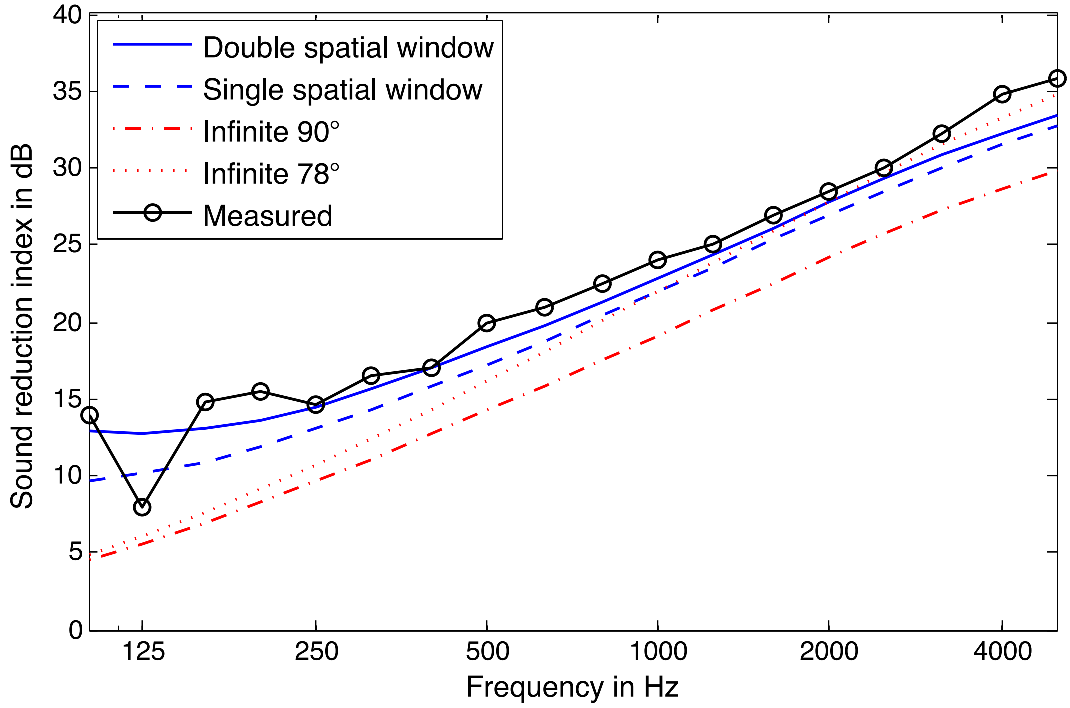

Figure 14: The sound reduction index of an aluminium plate. Measured data from Villot et al. [1]. The blue lines represents the spatially windowed system, with a single and a double window. The red lines represents the infinite system, one with reduced incident field diffusiveness.

single spatially window is to be used, but in this case, the double window gives better agreement with measurement data.

There is a slight deviation in reduction index between the measurement and the double spatial window in the highest frequency range. It would be interesting to compare them further up in frequency. The critical frequency of the plate is, as stated in table 2, $f_c = 10.9$ kHz. Unfortunately, the measurement data is only available in the range 100-5000 Hz.

8.1.2 Energy levels

In this section, the aluminium plate is put as the separating wall between two identical rooms. The SEA model of this system consists of three subsystems, as in figure 11. The parameters of the model are given in table 3. This is modelled in AutoSEA v. 1.5. The non-resonant transmission between the rooms is said to be due to the mass-law, with mass of the plate $m = 4.57$ kg.

Table 3: The parameters for the two rooms separated by a single aluminium plate in AutoSEA.

	Subsystem 1: sending room	Subsystem 2: receiving room	Subsystem 3: plate
Wave type	longitudinal	longitudinal	bending
Material	air	air	aluminium
Dimensions (m)	$1.4 \times 1.1 \times 2$	$1.4 \times 1.1 \times 2$	$1.4 \times 1.1 \times 0.0011$
DLF	$4.4/f$	$4.4/f$	0.01
Power input	0.005 W		

The system is also modelled with the implemented SEA model illustrated in figure 13, with transmission factor as in figure 14. In this model, only subsystem 1 and 2 in table 3 are included. The behaviour of the panel is given by the transmission factor.

Table 4: Frequency limits where the modal overlap factor is greater than 1, which is assumed in SEA. Also frequency limits where the mode count is greater than 2 and greater than 30 for 1/3 octave bands.

	Subsystem 1: sending room	Subsystem 2: receiving room	Subsystem 3: plate
MOF > 1	$f > 400$ Hz	$f > 400$ Hz	$f > 160$ Hz
Mode count > 2	$f > 160$ Hz	$f > 160$ Hz	$f > 25$ Hz
Mode count > 30	$f > 500$ Hz	$f > 500$ Hz	$f > 200$ Hz

The calculated energy levels in the sending and receiving room is seen in figure 15. Some measures of the lower frequency limit where SEA modelling is applicable is given in table 4. Above 500 Hz the modal overlap factor is greater than 1 and there are more than 30 modes per 1/3 octave band in every subsystem. So above this frequency, it is assumed that the SEA certainly is applicable. Above 160 Hz, there are more than 2 modes per 1/3 octave band in every subsystem, but the modal overlap factor is less than 1 for the two rooms. So in the range 160 Hz to 500 Hz, the SEA model is probably not as accurate.

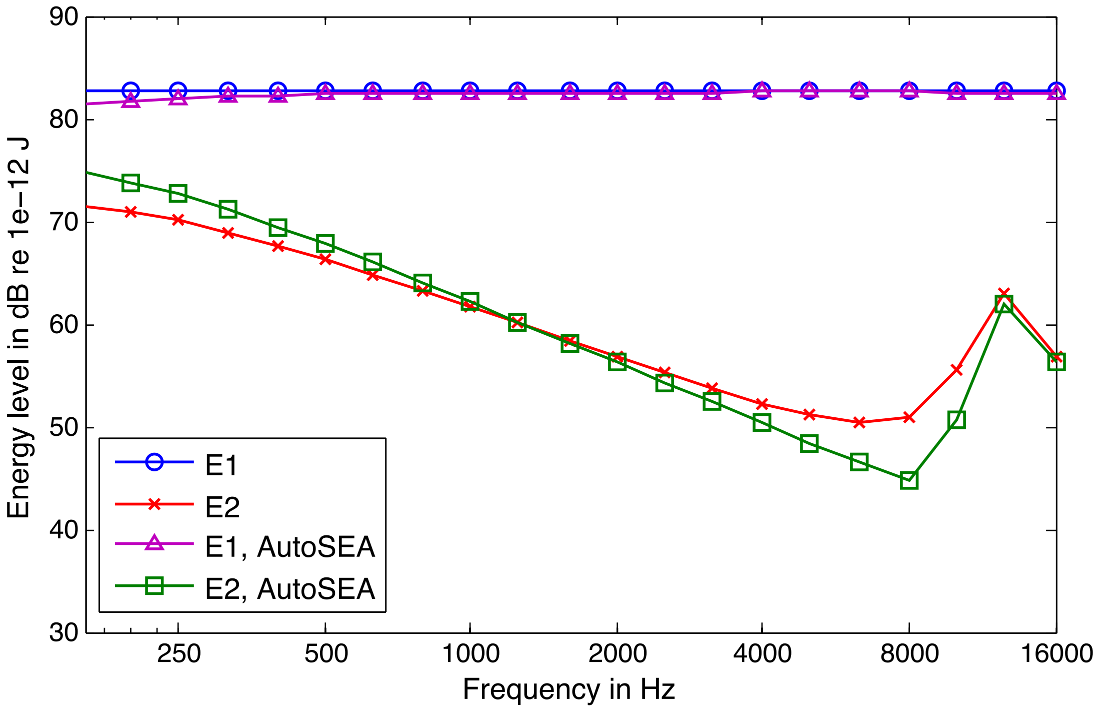

Figure 15: Energy level in the sending room (subsystem 1) and receiving room (subsystem 2), estimated with two different approaches. The implemented SEA model, with transmission factor calculated with a double spatial window, and also a SEA model as in figure 11, modelled in AutoSEA v.1.5.

Comparing the energy levels in figure 15 the predictions methods give a fairly similar result. Just below the resonance peak at about 11 kHz, there is some deviations in energy level in the receiving room. AutoSEA gives a lower energy level than the implemented SEA model. The slope of the energy level in the receiving room is also a bit different between the two methods.

At low frequencies, below 500 Hz, the energy level in the sending room is lower for AutoSEA. But as stated earlier, below 500 Hz, there is less than 30 modes per 1/3 octave band, which indicates that SEA might not be accurate. And below 400 Hz, the modal overlap factor is less than 1 in both rooms, which is an even stronger indicator that SEA is not applicable. If the modal overlap factor is less than 1, SEA usually overestimates the coupling loss factors [13]. This might be the reason why the energy level in the sending room drops below 400 Hz with AutoSEA.

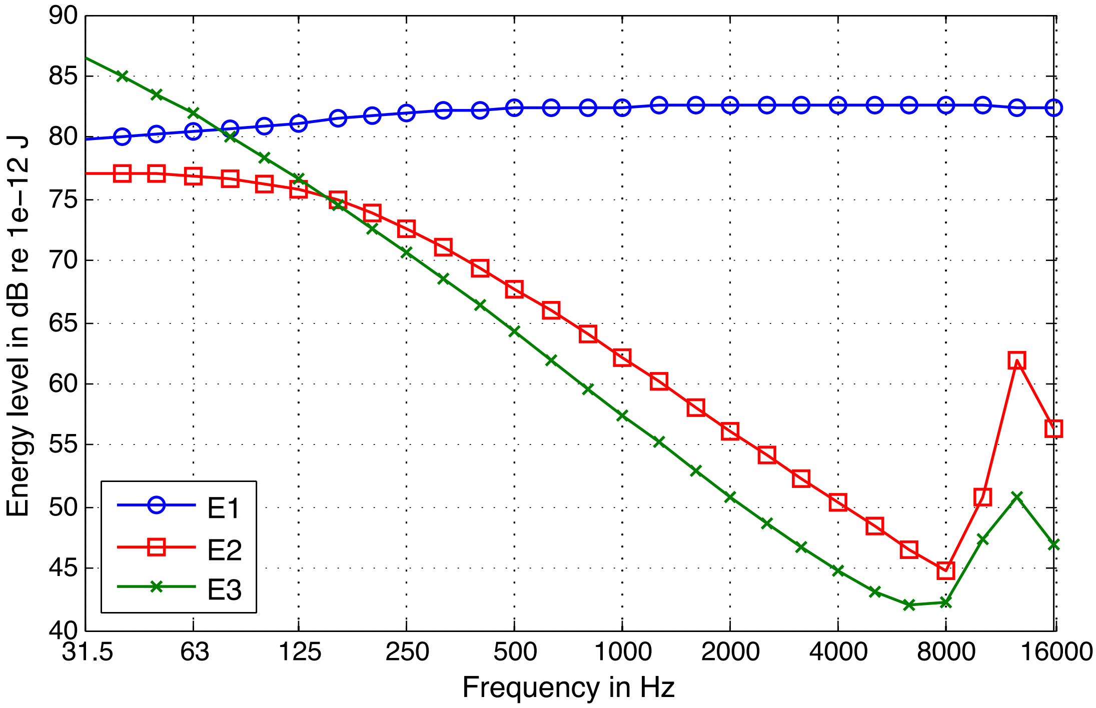

Figure 16: Energy levels for the SEA model in table 3 calculated in AutoSEA v. 1.5. Subsystem 1 is the sending room, subsystem 2 the receiving room, and subsystem 3 the aluminium plate.

But where does this energy go? The energy levels for all three subsystems calculated with AutoSEA are shown in figure 16. There is a tendency that the energy levels in both rooms drop at low frequencies, and the energy level increases at low frequencies in the plate. This gives further evidence that the coupling loss factors from the rooms are overestimated at low frequencies.

8.1.3 Power input to the receiving room

To further investigate the similarities and differences between AutoSEA and the implemented SEA model, the power input to subsystem 2, the receiving room, is compared. This can be seen in figure 17. The total power input for the implemented SEA model and AutoSEA is similar to the energy level in the sending room.

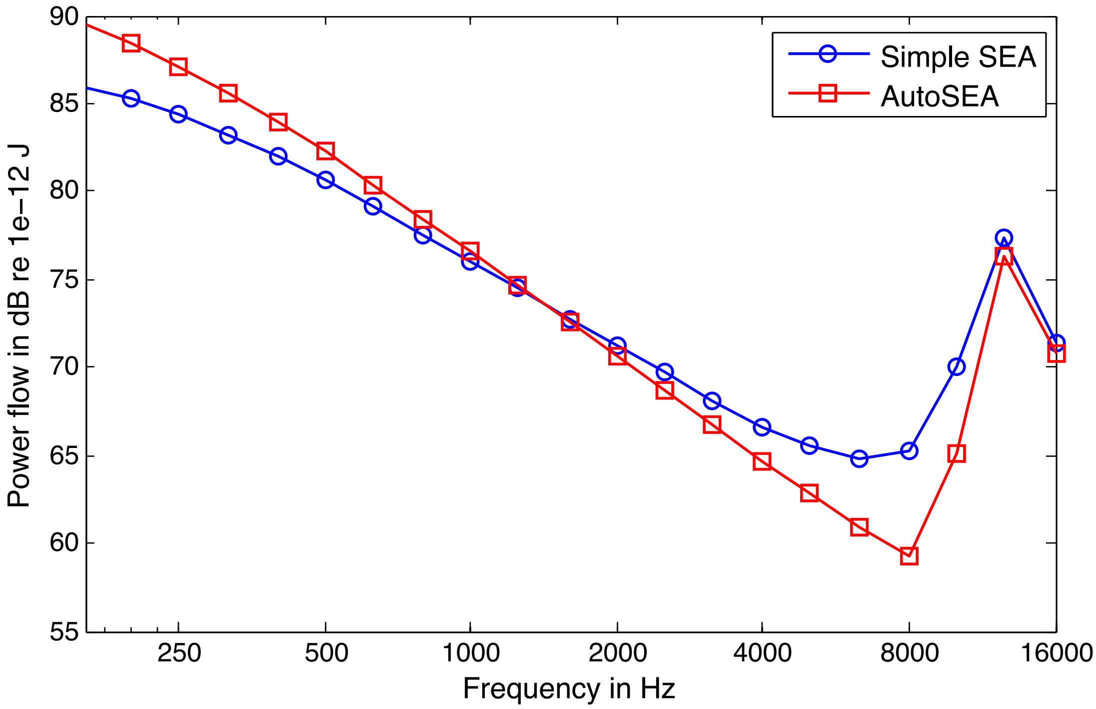

Figure 17: The total power input to the receiving room, subsystem 2 calculated with two different methods; The implemented SEA model with double spatially windowed transmission factor, and calculated with AutoSEA v. 1.5.

The total input power to the receiving room, calculated with AutoSEA is split up in its different contributions from the sending room and the plate. This is shown in figure 18. It clearly shows that below the critical frequency the power input mostly from the sending room, i.e. non-resonant transmission. The implemented SEA model is also used, with transmission factor from the diffuse field mass-law; $R_d = R_0 - 10\log_{10}(0.23R_0)$, where R_0 is the mass-law in its simplest form, $R_0 = 20\log_{10}(m''f) - 42.5$ dB. The non-resonant transmission is fairly similar to the diffuse field mass-law.

At 8 kHz the contribution from the plate, i.e. resonant transmission is noticed in the total power input to the receiving room. This gives a increase in energy level in the receiving room for frequencies around the critical frequency. For the energy level calculated with the implemented SEA model, this increase is noticed already at about 4 kHz, and the transition from non-resonant to resonant transmission is much smoother compared to AutoSEA. This is most likely due to the angle

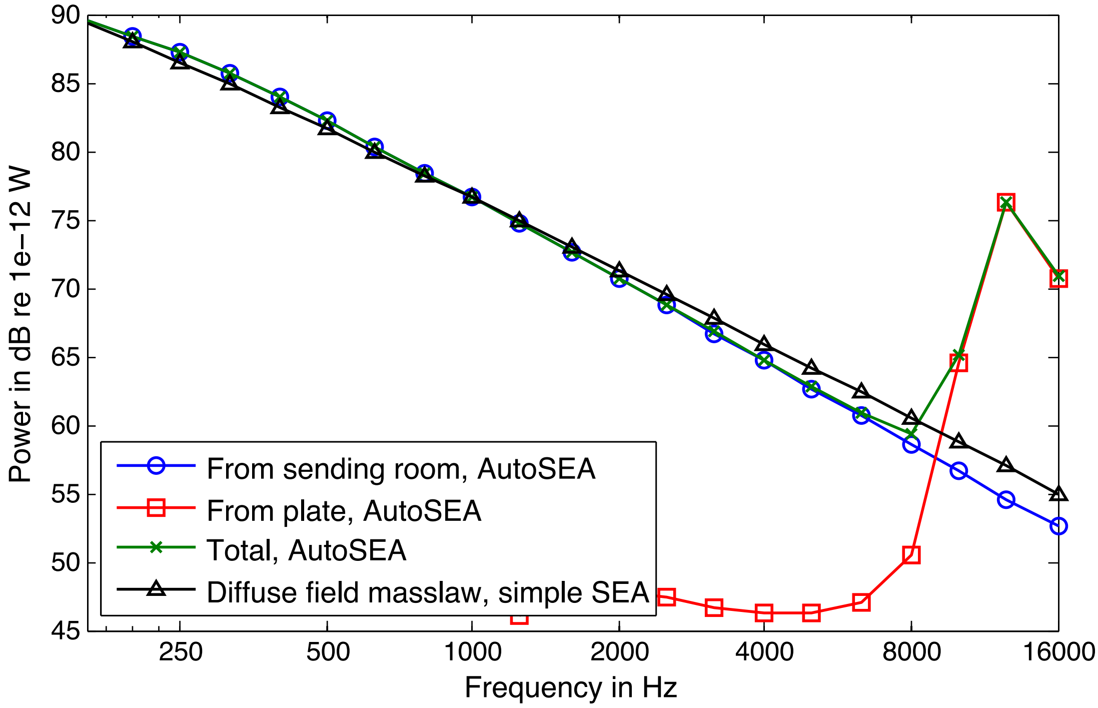

Figure 18: Power input to subsystem 2, the receiving room. The total power input is split up in its contributions from the sending room, non-resonant transmission, and from the plate, resonant transmission. The power input is also calculated with the implemented SEA model, with transmission factor from the diffuse field mass-law.

dependence in transmission factor.

8.1.4 The implemented SEA model

The implemented SEA model used in the calculations is compared with the same SEA model with two subsystems in AutoSEA. The transmission factor is calculated with a double spatial window and used as input in AutoSEA. In the SEA model, the sending and receiving room is modelled with parameters as in table 3. The resulting energy levels for both methods are shown in figure 19, and it shows that both prediction models basically give the same result. There is a tiny deviation of less than 1 dB for low frequencies.

In the MATLAB script, all coupling loss factors are calculated with equation 92. With the consistency relation, this indicates that the ratio of modal densities are equal to the ratio of the volume of the rooms,

$$\frac{n_1}{n_2} = \frac{V_1}{V_2}. \tag{97}$$

Looking at the expression for modal density of a room in table 1 this means that only the first term is used. In AutoSEA the full expression containing all three terms are used. This is the reason for the small deviation at low frequencies.

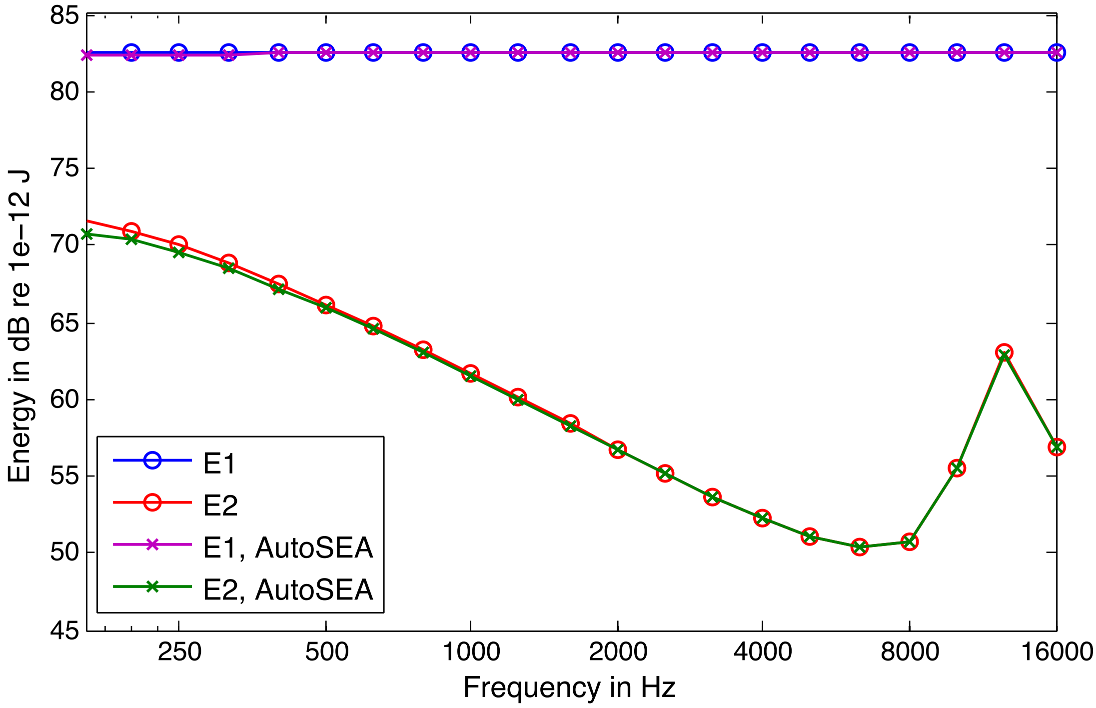

Figure 19: The energy levels in the sending room (subsystem 1) and receiving room (subsystem 2). Both methods uses the implemented SEA model, with a double spatially windowed transmission factor.

8.1.5 Radiation efficiency

The coupling loss factor calculated with AutoSEA can be used to estimate the radiation efficiency, by rearranging equation 88. This is shown in figure 20 together with the radiation efficiency $\sigma(k_p)$, which was calculated with equation 56. The two different radiation efficiency agree well. The ripple at low frequencies is due to the plate dimension L, which is included in equation 56.

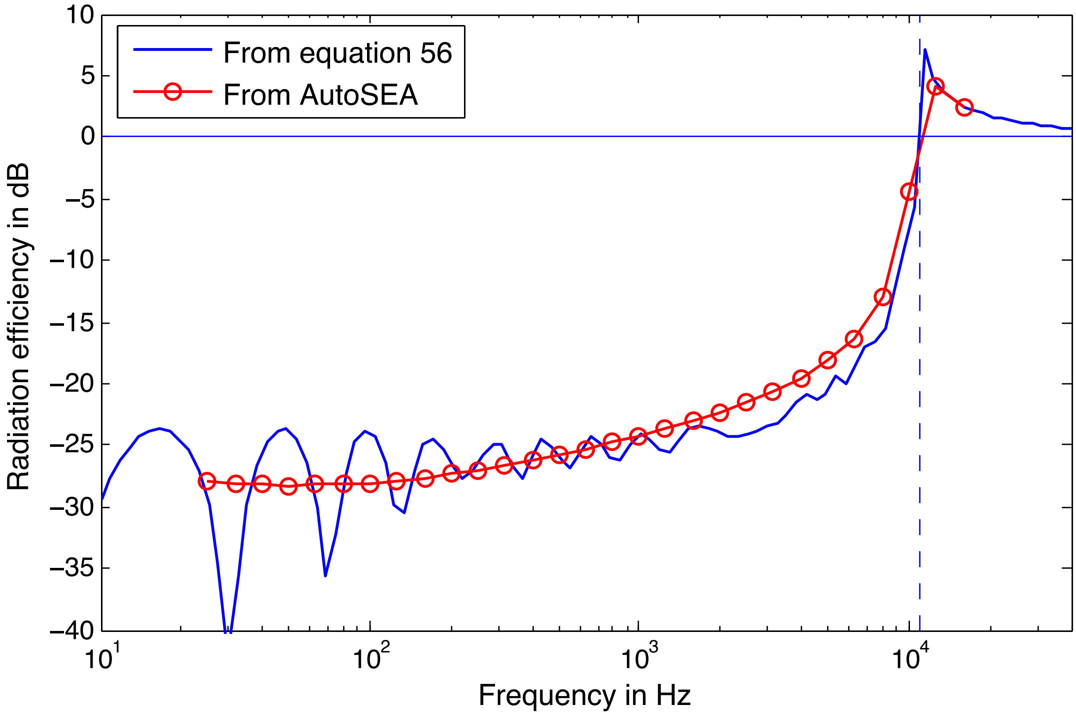

Figure 20: The radiation efficiency from the coupling loss factor between the plate and the receiving room, which was calculated in AutoSEA v. 1.5. Also the radiation efficiency $\sigma(k_p)$ calculated with equation 56.

8.2 Double glazing

A double glass window is now considered, with two identical glass panels separated by an air gap with depth $d = 12$ mm. The material data of the glass panel are given in table 2. The special frequencies for this double wall is given in table 5.

Table 5: Interesting frequencies of the double glazing. $f_{d=\lambda/6}$ is the frequency where one sixth of a wavelength fits the depth of the cavity, which is a common lower limit for diffuse field. Correspondingly, $f_{d=\lambda/2}$ is the frequency where half the wavelength fits the depth of the cavity. Above this frequency, modes can occur along the depth.

Double wall resonance	$f_0 = 244$ Hz
Critical frequency	$f_c = 3.18$ kHz
$\lambda/6 = d$	$f_{d=\lambda/6} = 4.76$ kHz
$\lambda/2 = d$	$f_{d=\lambda/2} = 14.2$ kHz

8.2.1 Transmission factor

The transmission factor of the double glazing is calculated as in section 7. A double spatial window with dimension $L = \sqrt{1.48 \times 1.23}$ m is applied to the transmission factor to take into account for the finite size of the structure. Damping in the cavity is included by a power attenuation coefficient $\gamma = 0.2$.

The reduction index of the structure is shown in figure 21. The first thing to notice is the dip at around 250 Hz, which is due to the double wall resonance. All prediction methods agree well with measurements here. The critical frequency of the glass panels is seen at 3150 Hz, and prediction methods give similar reduction index to the measured ones at this frequency. Apart from at those frequencies, the differences between the measured and predicted result are quite large. The infinite case, i.e the one without spatial window, fails to predict the reduction index in the range from the double wall resonance, $f_0 = 244$ Hz to the resonance frequency of the panels, $f_c = 3180$ Hz. The spatially windowed cases give a better agreement with the measurements, especially the double spatial window. The infinite case where the diffusiveness is reduced to 78° gives a strange result.

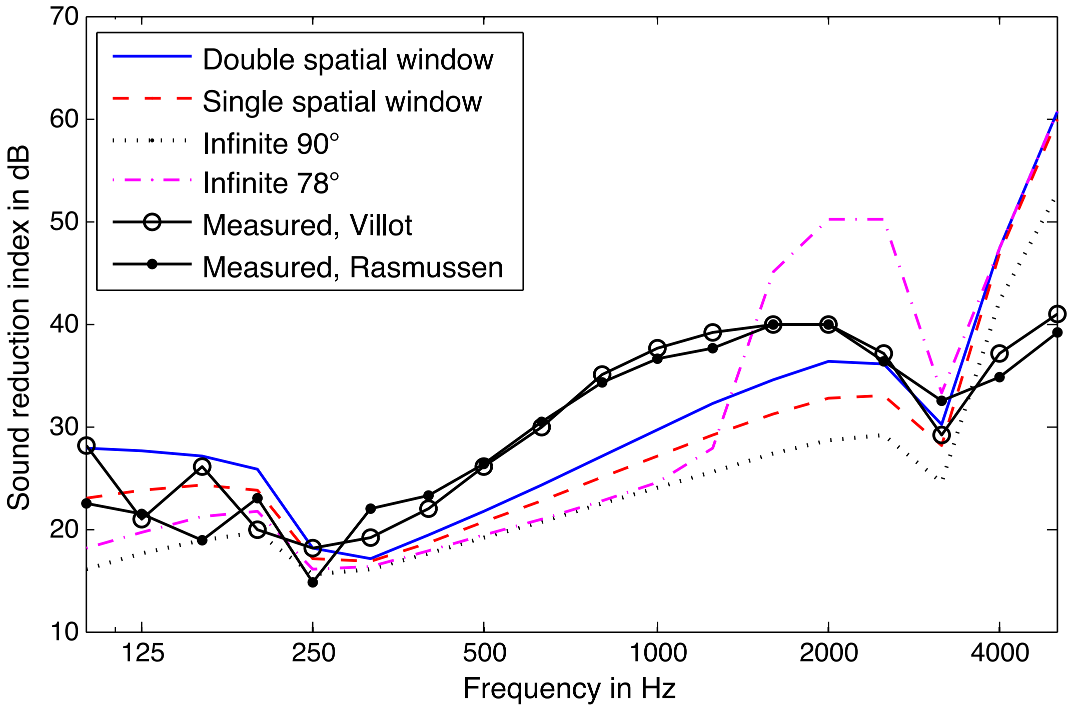

Figure 21: The sound reduction index of a double glass panel. Measured data from Villot et al. [1], and Rasmussen [2]. The blue line and the red dashed line represents the spatially windowed system, with a single and a double window. The black dotted line and the purple dash-dotted line represents the infinite system, one with reduced incident field diffusiveness.

It seems as the double spatially windowed transmission factor agree best with measurements in this case as well. But there is a difference in reduction index of at most 10 dB compared to the measured values. So when plugging in this transmission factor in the implemented SEA model, the energy level in the receiving room is probably overestimated.

The double spatial window is compared with the empirical model by Sharp, equation 15, discussed in section 2.2. This is shown in figure 22, which also shows the reduction index calculated with transfer matrices, but with wave propagation in the air cavity normal to the panels, i.e. letting $\theta = 0$ in the transfer matrix of the air cavity, equation 33. This gives a much larger reduction index compared to the nominal model, but as seen in figure 22 this corresponds quite well with Sharp.

Letting $\theta = 0$ in the transfer matrix of the air cavity leads to highest possible stiffness of the air cavity, leading to a higher reduction index than the nominal case. Figure 22 indicates that the model by Sharp is based on the same condition, with wave propagation normal to the panels in the air cavity.

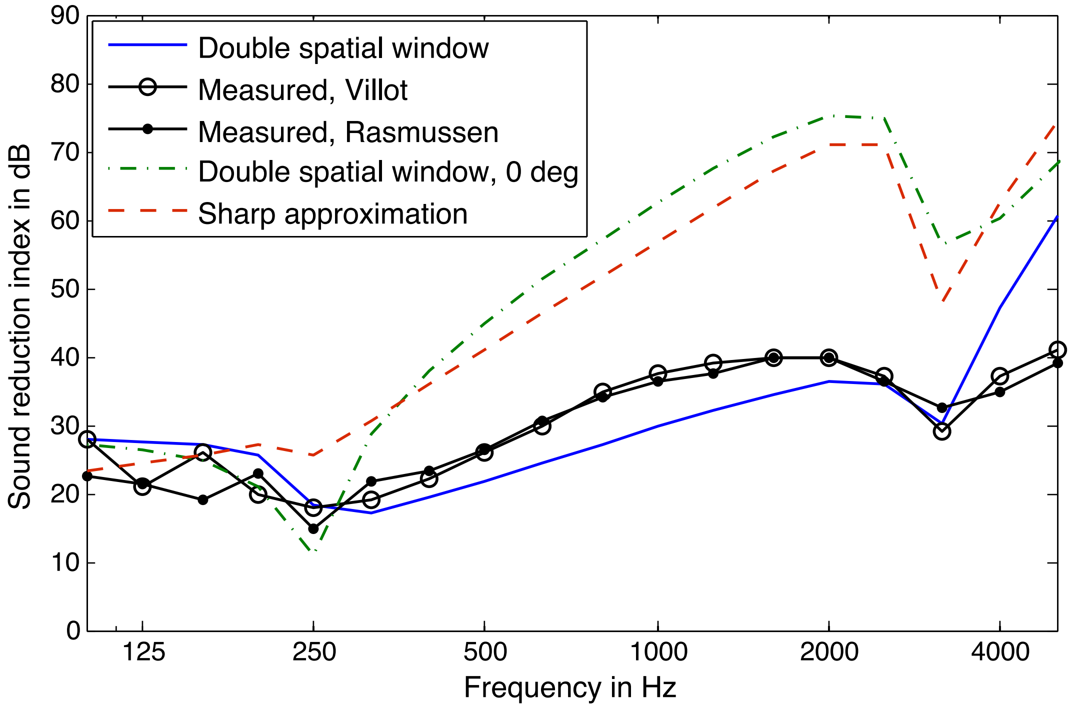

Figure 22: The sound reduction index of a double glass panel. Measured data from Villot et al. [1], and Rasmussen [2]. The blue line represents the spatially windowed system, with a double window. The red dashed line is calculated in the same way as the blue line, but with wave propagation normal to the panels in the air cavity, i.e $\theta = 0$ for all angles of incidence. The green dash-dotted line are calculated with formulas in SS-EN 12354-1 [6] and the empirical model by Sharp, equation 15.

8.2.2 Energy levels

In this section, the double glass panel is put as the separating wall between two identical rooms. The SEA model of this system consists of five subsystems, as in figure 12. The parameters of the model are given in table 6. This is modelled in AutoSEA v. 1.5. The non-resonant transmission between the sending room and cavity, and the cavity and receiving room is said to be due to the mass-law, with mass of the panels $m = 18.2$ kg.

Table 6: The parameters for the double glazing model in AutoSEA.

	Subsystem 1 & 2: rooms	Subsystem 3: cavity	Subsystem 4 & 5: panels
Wave type	longitudinal	longitudinal	bending
Material	air	air	glass
Dimensions (m)	$1.48 \times 1.23 \times 2$	$1.48 \times 1.23 \times 0.012$	$1.48 \times 1.23 \times 0.004$
DLF	$4.4/f$	$c_0\gamma/\omega$	0.05
Power input	0.005 W (subsys. 1)		

Table 7: Frequency limits where the modal overlap factor is greater than 1, which is assumed in SEA. Also frequency limits where the mode count is greater than 2 and greater than 30 for 1/3 octave bands.

	Subsystem 1 & 2: rooms	Subsystem 3: cavity	Subsystem 4 & 5: panels
MOF > 1	$f > 400$ Hz	$f > 1000$ Hz	$f > 160$ Hz
Mode count > 2	$f > 160$ Hz	$f > 315$ Hz	$f > 63$ Hz
Mode count > 30	$f > 500$ Hz	$f > 1250$ Hz	$f > 1000$ Hz

The applicability of this SEA model is first investigated by looking at the modal overlap factor and mode count, which is given in table 7. Since the separating panel is fairly small, and the air cavity has a low damping loss factor, the lower frequency limit is quite high. The condition of a modal overlap factor greater than 1 is fulfilled for all subsystems above 1 kHz. And the condition of more than 2 modes per 1/3 octave band is fulfilled above 315 Hz.

Figure 23 shows the energy levels in the sending and receiving room calculated with two different methods. The result from AutoSEA is compared to the implemented SEA model, with measurement data of the reduction index. The AutoSEA model has two different cases; At low frequencies, the wavelength is much larger than the depth of the cavity and thus it is modelled as a two-dimensional cavity. For higher frequencies wave propagation occurs in all three dimensions of

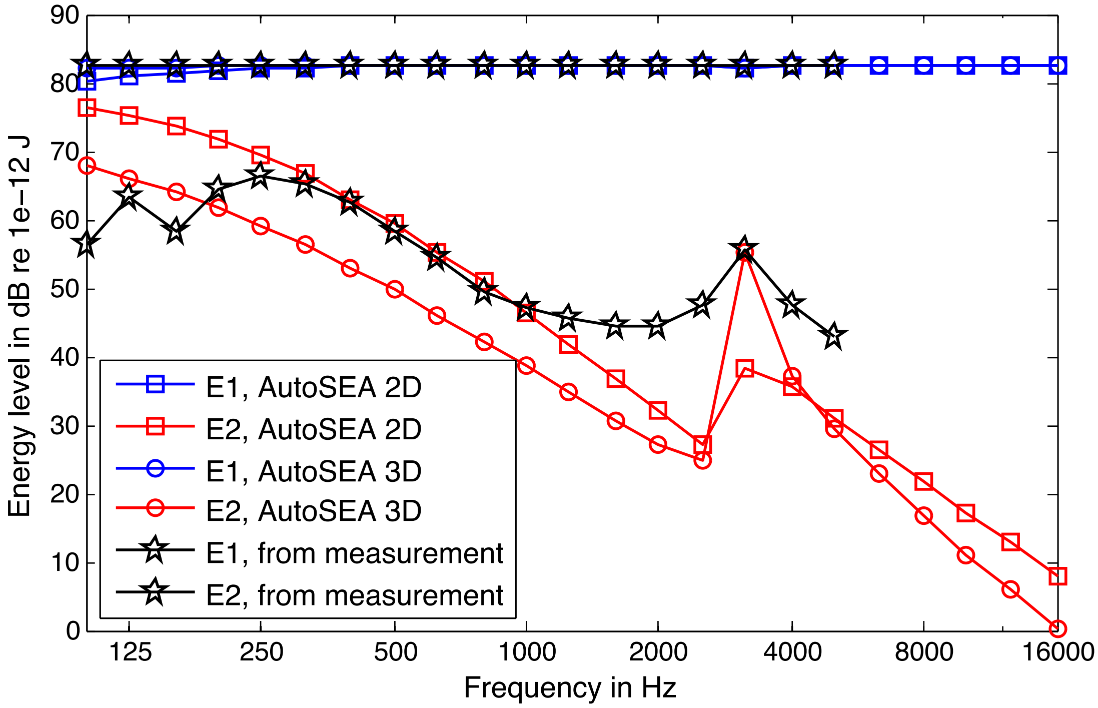

Figure 23: Energy levels of the sending and the receiving room separated by a double glazing, calculated with AutoSEA v. 1.5. In 2D case, the cavity is modelled as a 2D cavity, and in the 3D case it is modelled as a 3D cavity. The energy levels are also calculated with the implemented SEA model, using measurement data of sound reduction index from Villot et al. [1].

the cavity and thus it is modelled as a three-dimensional cavity. The transition between a two-dimensional and three-dimensional model lies somewhere around $f_{d=\lambda/6} = 4.76$ kHz and $f_{d=\lambda/2} = 14.2$ kHz. Comparing the two cases in figure 23, it seems as the 3D model best describes the system above 2.5 kHz, which is a bit lower than $f_{d=\lambda/6}$.

The energy level in the receiving room from AutoSEA is chosen to

$$E_2 = \begin{cases} E_{2,2D}, & \text{for } f \leq 2500 \text{ Hz} \\ E_{2,3D}, & \text{for } f > 2500 \text{ Hz}, \end{cases} \tag{98}$$

and this is displayed in figure 24 together with the energy level in the receiving room calculated with other methods. AutoSEA agrees well with the energy level that is based on a measurement of reduction index in the range from the double

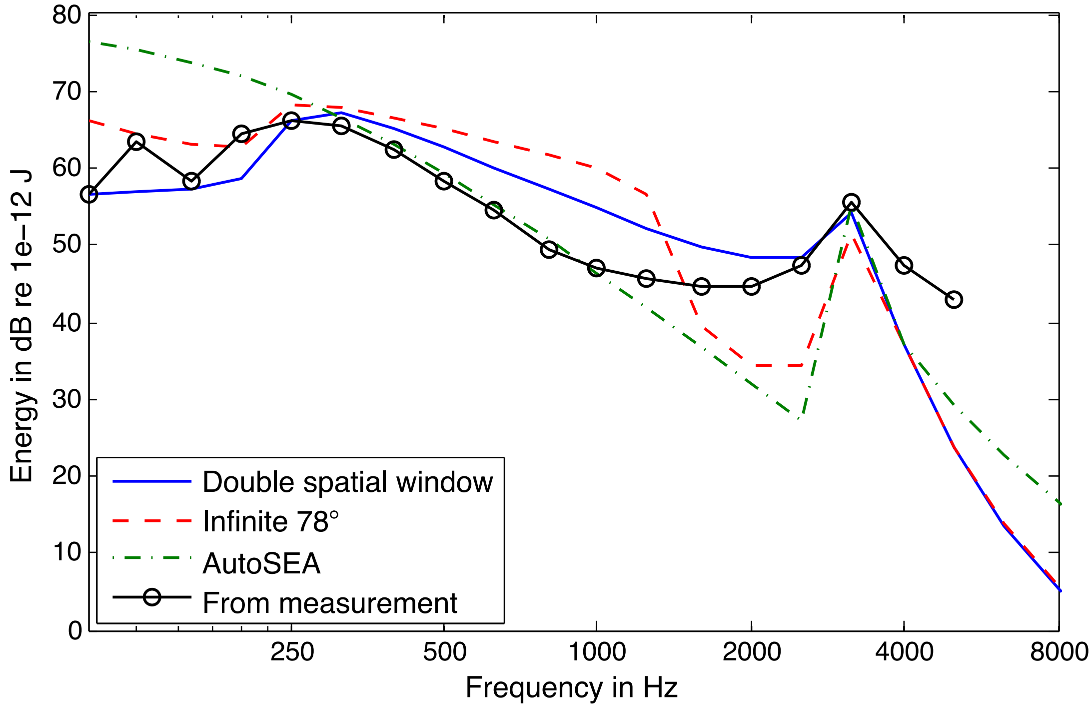

Figure 24: Energy level of the receiving room. The blue line represents the double spatially windowed case, the red dashed line the infinite structure with reduced incident field diffusiveness to 78°, the green dash-dotted line from AutoSEA v. 1.5 and the black circles the implemented SEA model with measurement data of sound reduction index from Villot et al. [1].

wall frequency up to 1 kHz. Below 315 Hz there are less than 2 modes per 1/3 octave band, which indicates that SEA is not reliable. Moreover, the non-resonant transmission that dominates in this frequency region is based on the mass-law, which means that the behaviour of the wall at low frequencies is not correctly modelled.

Above 1 kHz, AutoSEA declines in comparison with the measurement, similar to the single aluminium plate. But in this region AutoSEA agrees fairly well with the case with a transmission factor without spatial window, but with reduced incident field diffusiveness. The double spatial window do not agree at all with AutoSEA in pretty much the whole frequency range.

8.2.3 Radiation efficiency

The coupling loss factor calculated with AutoSEA is used to estimate the radiation efficiency, by rearranging equation 88. The CLF between the second panel and the receiving room is identical in the 2D and 3D model.The radiation efficiency is shown in figure 25, together with the radiation efficiency $\sigma(k_p)$, which was calculated with equation 56. The two different radiation efficiency agree well. Just as the radiation efficiency of the aluminium panel, ripple is seen at low frequencies. This is due to the plate dimension L, which is included in equation 56.

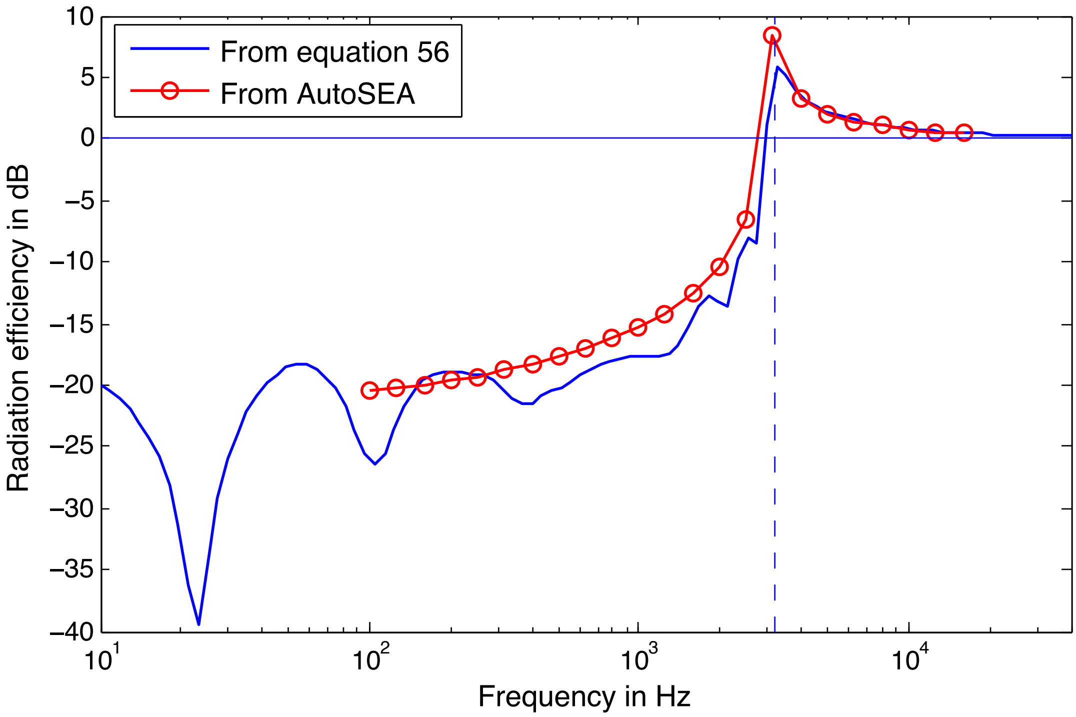

Figure 25: The radiation efficiency from the coupling loss factor between the second plate and the receiving room, which was calculated in AutoSEA v. 1.5. Also the radiation efficiency $\sigma(k_p)$ of a glass panel calculated with equation 56.

8.3 Double gypsum wall

In this section, a double gypsum wall is the separating element between two identical rooms. The SEA model is as in figure 12, with parameters given in table 8. As in the previous cases, the transmission factor, calculated with transfer matrices, and spatially windowed with a double window, is used to estimate the coupling loss factors in the implemented SEA model illustrated in figure 13. This is compared to the conventional model in AutoSEA. The calculations are performed with two different cavity depths, $d = 50$ mm and $d = 100$ mm, and with two different cavity damping, $\eta_{3d} = 0.01$ and $\eta_{3d} = 0.1$.

Table 8: The parameters for the model of two rooms separated by a double gypsum wall in AutoSEA.

	Subsystem 1 & 2: rooms	Subsystem 3: cavity	Subsystem 4 & 5: panels
Wave type	longitudinal	longitudinal	bending
Material	air	air	gypsum
Dimensions (m)	$3 \times 3 \times 4$	$3 \times 3 \times d$	$3 \times 3 \times 0.01$
DLF	$4.4/f$	η_{3d}	0.05
Power input	0.005 W (subsystem 1)		

Table 9: Frequency limits where the modal overlap factor is greater than 1, which is assumed in SEA. Also frequency limits where the mode count is greater than 2 and greater than 30 for 1/3 octave bands.

	Subsystem 1 & 2: rooms	Subsystem 3: cavity	Subsystem 4 & 5: panels
MOF > 1	$f > 125$ Hz	$f > 500$ Hz ($\eta_{3d} = 0.01$) $f > 160$ Hz ($\eta_{3d} = 0.1$)	$f > 160$ Hz
Mode count > 2	$f > 80$ Hz	$f > 160$ Hz	$f > 25$ Hz
Mode count > 30	$f > 250$ Hz	$f > 630$ Hz	$f > 200$ Hz

The lower limits for SEA applicability of this system is given in table 9. The cavity with damping $\eta_{3d} = 0.01$ has a lower frequency limit of 500 Hz where the modal overlap is greater than 1. And the mode count is more than two for frequencies above 160 Hz. When the damping loss factor is increased to $\eta_{3d} =$

0.1 modal overlap factor is greater than 1 for frequencies above 160 Hz. Some interesting frequencies of this double wall is given in table 10.

Table 10: Insteresting frequencies of the double gypsum wall. $f_{d=\lambda/6}$ is the frequency where one sixth of a wavelength fits the depth of the cavity, which is a common lower limit for diffuse field. Correspondingly, $f_{d=\lambda/2}$ is the frequency where half the wavelength fits the depth of the cavity. Above this frequency, modes can occur along the depth.

	$d = 50$ mm	$d = 100$ mm
Double wall resonance	$f_0 = 130$ Hz	$f_0 = 92$ Hz
Critical frequency	$f_c = 2.82$ kHz	$f_c = 2.82$ kHz
$\lambda/6 = d$	$f_{d=\lambda/6} = 1.1$ kHz	$f_{d=\lambda/6} = 570$ Hz
$\lambda/2 = d$	$f_{d=\lambda/2} = 3.4$ kHz	$f_{d=\lambda/2} = 1.7$ kHz

8.3.1 Comparison of different cavity depths

Two different cavity depths are compared in figure 26, which shows the energy level in the receiving room. The cavity is modelled as a 3D cavity in AutoSEA at high frequencies. This is indicated by the dashed lines. They are plotted for frequencies above $f_{d=\lambda/6}$.

The double wall resonance seems to be correctly described by the implemented SEA model for the two different depths. The critical frequency as well, the peak in energy level is at the critical frequency in both cases. Above the critical frequency, there are some resonance behaviour, which is most likely due to modes along the depth of the cavity. The energy level is not really affected by the depth of the cavity in this frequency range. However, at frequencies between the double wall resonance and the critical frequency, there is about 5 dB difference in energy level between the two depths. The same difference is seen in AutoSEA.

From about 500 Hz up to the critical frequency there is a large deviation between the implemented SEA model and AutoSEA. Bearing in mind that the transmission factor was underestimated between f_0 and f_c in comparison with measured values, and the dip in energy level below the critical frequency was exaggerated for AutoSEA in comparison with the measured values, the true energy level probably lies somewhere in between these two cases. However, from figure 26 one can conclude that the implemented SEA model responds to changes in cavity depth in a similar manner as AutoSEA.

It could be noted that even though the modal overlap factor is less than 1 in the cavity below 500 Hz, AutoSEA seems to give reliable result further down in frequency.

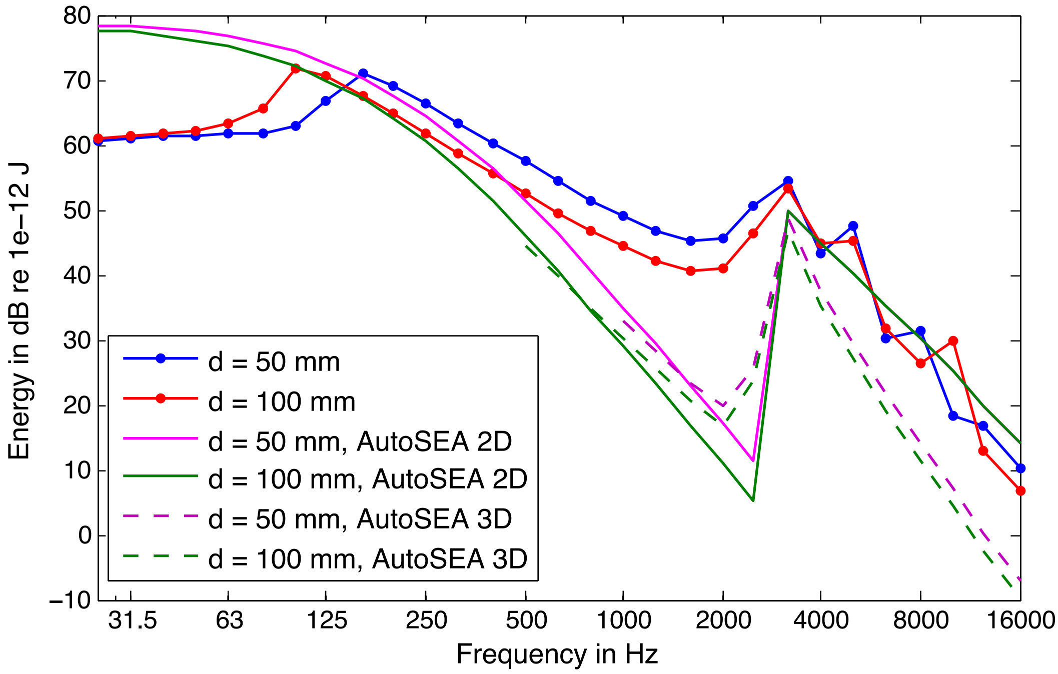

Figure 26: The energy level in receiving room, for two different cavity thickness. The DLF of the cavity is 1% in both cases. Three different models has been used; The implemented SEA model, AutoSEA v. 1.5 with the cavity modelled as two-dimensional and AutoSEA v. 1.5 with the cavity modelled as three-dimensional.

8.3.2 Comparison of different cavity damping

Two different cavity damping are compared in figure 27, which shows the energy level in the receiving room. The depth of the cavity is $d = 100$ mm in both cases. The dashed lines represents the case with a 3D cavity, and they are plotted for frequencies above $f_{d=\lambda/6}$.

The energy level decreases when the damping increases in both cases. This seems to be correct since more energy is dissipated in the cavity. For high frequencies, the resonance peaks in the implemented SEA model are attenuated when the damping is increased, which also seems sensible. Between the double wall resonance and the critical frequency, the highly damped case is about 3 dB lower than the lightly damped case, for the implemented SEA model. In AutoSEA, however, there is about 10 dB difference between the two cases.

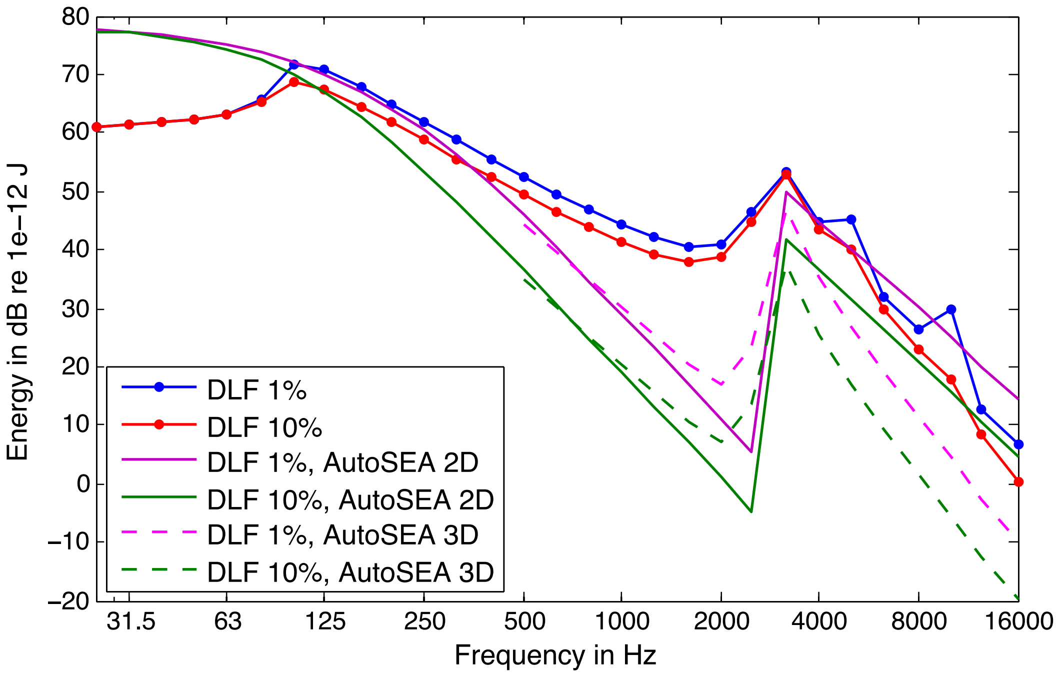

Figure 27: The energy level in receiving room, for two different cavity DLF. The depth of the cavity is 100 mm in both cases. Three different models has been used; The implemented SEA model, AutoSEA v. 1.5 with the cavity modelled as two-dimensional and AutoSEA v. 1.5 with the cavity modelled as three-dimensional.

9 Discussion

Three different systems have been used to validate the result, the single aluminium plate, the double glazing and the double gypsum wall. In this section, the result is summarised and discussed.

Single aluminium plate

The transmission factor for a single aluminium plate is calculated with the transfer matrix method, and compared to measurement data. Different versions of the spatially windowing technique are compared and it is concluded that the double spatial window gives best agreement with the measurement data. Compared to the method of reducing the diffusiveness of the incidence wave field to 78°, the double spatial window is proven to give better agreement in the whole frequency range. Reducing the diffusiveness gives a steeper slope, which gives good agreement in the high frequency range.

The calculated transmission factor is used to calculate the coupling loss factors in the implemented SEA model. The energy levels are compared with a conventional single wall model in AutoSEA v. 1.5, and good agreement is obtained. The slope of the energy level in the receiving room is somewhat steeper in AutoSEA, and the transition from non-resonant to resonant transmission is smoother in the implemented SEA model.

By looking at the power input to the receiving room in AutoSEA it is seen that the non-resonant transmission corresponds to the diffuse field mass-law. The resonant transmission is only contributing to the total transmission at high frequencies, and this transition from non-resonant to resonant transmission is very sudden. The transmission factor is calculated for every incidence angle with the transfer matrix method. Since there are always some angle where the transmission is high, integrating over all angles gives this smooth transition from non-resonant to resonant transmission.

The implemented SEA model with two subsystems is also modelled in AutoSEA, with the transmission factor as input. They give identical result, except for very low frequencies, where AutoSEA drops in comparison with the model in MATLAB and it is concluded that this difference is due to that AutoSEA uses all three terms in the expression for modal density of the rooms, whereas in the

MATLAB script, only the first term is used.

Double glazing

The transmission factor for a double glazing calculated with the transfer matrix method shows poor agreement with measurement data in the frequency region above the double wall resonance and below the critical frequency. The spatially windowing technique improves the result substantially, but not enough. The reduction index is lower than the measured case. The trick of reducing the diffusiveness of the incidence wave field to 78° gives a strange result, that does not agree with the measurement data.

The reduction index is also compared with the model by Sharp, and it is shown that it gives a much higher reduction index in the frequency range from the double wall resonance and up. Compared to the model by Sharp, the implemented MATLAB script seems to model the reduction index quite well, and it has the advantage that it is conservative, i.e. it underestimates the reduction index.

By forcing the waves in the cavity to propagate normal to the panels for all angles of incidence, i.e. letting the angle $\theta = 0$ in the transfer matrix of the air cavity, a model that agrees fairly well with Sharp is obtained. This probably means that the model by Sharp is based on wave propagation normal to the panels in the air cavity.

The transmission factor is used in the implemented SEA model to compare the method with AutoSEA v. 1.5. Comparing AutoSEA with measured values of transmission factor, they are similar from the double wall resonance up to about 1 kHz. Between 1 kHz and the critical frequency of 3.18 kHz there is a smooth transition from non-resonant to resonant transmission for the measured values. The effect of the resonant transmission in AutoSEA is not noticed until 2.5 kHz, where it fully takes over the transmission. This gives a much lower dip in energy level for AutoSEA compared to the measured values.

The implemented SEA model with a transmission factor with reduced incident field diffusiveness shows the same dip in energy level as AutoSEA, just below the resonance frequency. This is probably because the non-resonant transmission through the two panels in AutoSEA is modelled with the diffuse field mass-law, which is tuned to agree with measurement data, in the same way as the reduced diffusiveness is tuned to 78° to obtain the same agreement.

The transmission factor from the transfer matrix method with a double spatial window gave a lower reduction index compared to measurement data, which indicates that the energy level in the receiving room is too high with the implemented SEA model. This is shown to be the case. However, one thing that could be noted in the low frequency range is that the energy level seems to be correctly described around the double wall resonance. This is not the case in AutoSEA, which only uses the mass-law to describe the transmission at low frequencies.

Double gypsum wall

For the double gypsum wall, no measurement data of reduction index is available. The energy levels where calculated with the implemented SEA model and compared with AutoSEA for two different cavity depths and two different cavity damping. As for the double glazing, large differences in energy levels is seen. At the double wall resonance the energy level is similar for both methods, but as the frequency goes up AutoSEA drops much in comparison with the implemented SEA model. The true energy level most likely lies between these two curves.

However, it is seen that the implemented SEA model and AutoSEA responds similarly to a change in cavity depth. And for the implemented SEA model, the double wall resonance is shifted down in frequency when the depth of the cavity is increased, which is expected. Above the critical frequency the resonance peaks present in the implemented SEA model are shifted when the depth of the cavity is changed.

Comparing different cavity damping there are differences between AutoSEA and the implemented SEA model. The energy level is decreased by about 10 dB when the damping is increased in AutoSEA. In the implemented SEA model, the decrease is about 3 dB for frequencies between the double wall resonance and the critical frequency. Above the critical frequency, the resonance peaks are attenuated, which seems reasonable.

9.1 Limitations of the method

The transfer matrix method used in this thesis provides a relation of the pressure and particle velocity on both sides of an infinite layer. The finite size of the structure is taken into account by applying a spatial window on the incidence wave field and the vibration velocity field of the infinite structure before calculating the radiated field. This is of course an approximation, but it seems to describe the transmission of a plate with high accuracy. However, this method seems to be giving an incorrect description of the wave field in the cavity, which results in a underestimated reduction index. A possible reason for this is that reflections from the edges of the cavity is not included since the cavity is of infinite size. Another reason might be that the transmission factor is calculated for each angle separately, and the contribution from each angle is summed in an integral.

10 Conclusion

The transfer matrix method together with the spatial windowing technique gives good agreement of reduction index with measured data, in the case of a single plate. The implemented SEA model agrees with AutoSEA v. 1.5, and it is concluded that the implemented SEA model gives a more detailed result. The transition from non-resonant to resonant transmission is smoother in the implemented SEA model, which seems realistic. It would have been interesting to study multilayered plates as well.

The transfer matrix method underestimates the reduction index of a cavity wall between the double wall resonance and the critical frequency. The result is improved with the spatially windowing technique, but a good agreement with measurement data is not obtained. Reducing the diffusiveness of the incidence wave field does not provide satisfactory result either. Compared to the model by Sharp, the implemented model appears as a qualified conservative model, since Sharp gives a very exaggerated reduction index compared to measurements.

The reduction index is underestimated between the double wall resonance and the critical frequency. Together with the implemented SEA model, the energy level in the receiving room is overestimated. Comparing with AutoSEA v. 1.5 the deviation in energy level is large in this frequency region. However, comparing with measurements AutoSEA gives a much lower energy level below the critical frequency. Hence it does not seems as if AutoSEA gives sufficient agreement either.

10.1 Suggestions for future work

The method agreed well with measurements and AutoSEA for a single plate, but underestimates the reduction index for cavity walls (i.e a double wall), and it was concluded that it is probably due to the model of the air cavity. One thing that could be investigated is if the model is suitable for other multilayered elements excluding cavity walls. On example of this a sandwich construction.

Further, the transfer matrix modelling could be extended to include other elements such as a solid layer or a porous layer with elastic frame. Both types requires more than two variables to describe the acoustic wave field, giving larger transfer matrices than 2×2. It would also be interesting to investigate if flanking transmission could be included in the implemented SEA model by means of transfer matrices.

Finally, the validation could be extended to include more setups. It would also be beneficial to conduct measurements to validate the method further. Also to investigate the range of applicability, both in terms of frequency and layer thickness.

References

[1] M. Villot, C. Guigou, and L. Gagliardini. Predicting the acoustical radiation of finite size multi-layered structures by applying spatial windowing on infinite structures. *Journal of Sound and Vibration*, 245(3):433–455, 2000.

[2] T. E. Vigran. Predicting the sound reduction index of finite size specimen by a simplified spatial windowing technique. *Journal of Sound and Vibration*, 325:507–512, 2009.

[3] M. L. Munjal. *Acoustics of ducts and mufflers with application to exhaust and ventilation system design.* John Wiley & Sons, 1987.

[4] T. E. Vigran. *Building Acoustics.* Taylor & Francis, 2008.

[5] M. J. Crocker and A. J. Price. Sound transmission using statistical energy analyis. *Journal of Sound and Vibration*, 9(3):469–486, 1969.

[6] Byggstandardiseringen, BST. *SS-EN 12354-1. Building acoustics - Estimation of acoustic performance of buildings from the performance of elements - Part 1: Airborne sound insulation between rooms*, 2000.

[7] B. H. Song and J. S. Bolton. A transfer-matrix approach for estimating the characteristic impedance and wave numbers of limp and rigid porous materials. *J. Acoust. Soc. Am.*, 107(3):1131–1152, 2000.

[8] J.-F. Allard and N. Atalla. *Propagation of sound in porous media : modelling sound absorbing materials.* John Wiley & Sons, second edition, 2009.

[9] R. Panneton. Comments on the limp frame equivalent fluid model for porous media. *J. Acoust. Soc. Am.*, 122(6):EL217–EL222, 2007.

[10] B. Brouard, D. Lafarge, and J.-F. Allard. A general method of modelling sound propagation in layered media. *Journal of Sound and Vibration*, 183(1):129–142, 1995.

[11] K. A. Mulholland, H. D. Parbrook, and A. Cummings. The transmission loss of double panels. *Journal of Sound and Vibration*, 6(3):324–334, 1967.

[12] L. Cremer, M. Heckl, and B. A. T. Petersson. *Structure-Borne Sound : Structural Vibrations and Sound Radiation at Audio Frequencies*. Springer Berlin Heidelberg, 3rd edition, 2005.

[13] R. J. M. Craik. *Sound transmission through buildings using statistical energy analysis*. Gower Publishing, 1996.

[14] D. Johansson and P. Comnell. Statistical energy analysis software : Development and implementation of an open source code in matlab/octave. Master's thesis, Chalmers University of Technology, 2010.